ISSN : 0973-0613

JOURNAL OF Wind and Engineering

Vol. 6 No. 2 July 2009

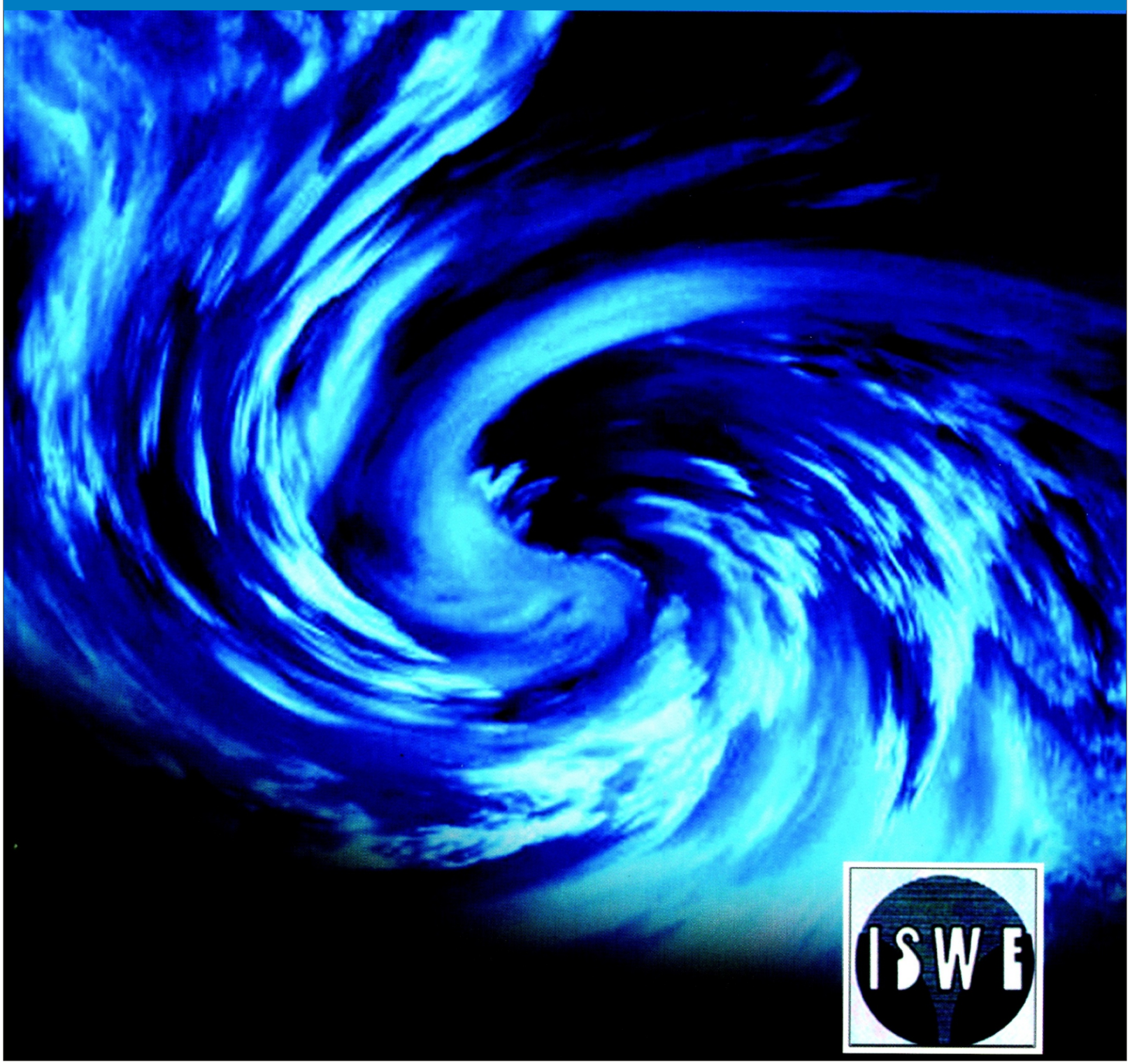

Journal of Wind and Engineering

Editor-in-Chief

Editors

International Review Board

JOURNAL OF WIND & ENGINEERING

Vol. 6 **No. 2** **July 2009**

CONTENTS

Journal of Wind and Engineering, Vol. 6, No. 2, July 2009, pp. 1-18

SHAPE EFFECTS ON THE WIND-INDUCED RESPONSE OF HIGH-RISE BUILDINGS

Ryan Merrick[1] and Girma Bitsuamlak[2]

[1] Technical Coordinator, RWDI Inc., Guelph, Ontario, Canada, email: Ryan.Merrick@rwdi.com
[2] Assistant professor, Department of Civil and Environmental Engineering/International Hurricane Research Center, Florida International University, Miami, Florida, 33174, email: bitsuamg@fiu.edu

ABSTRACT

This paper explored the effect of building shape on the wind-induced response of a structure through a comprehensive investigation of wind tunnel studies performed at Rowan Williams Davies and Irwin, Inc. (RWDI). The study focused on buildings with foot prints of square, circular, triangular, rectangular and elliptical shapes. Seed buildings were selected from an inventory of structures previously tested in a low-speed boundary layer wind tunnel (BLWT). The measured wind tunnel data for each of the sample seeds were factored to match a representative building shape at full scale for comparison purposes. Load patterns attributed to the cross-sectional shape of the structure were observed in the results. To provide a baseline value for the wind loads, the computed responses for the seeds were compared against the values given by the 2005 National Building Code of Canada (NBCC) and the American Society of Civil Engineers (ASCE) 7-05 Standard. The base load comparisons illustrated how certain building shapes perform in wind events.

Key words: shape effects, bluff bodies, base loads, tall buildings, wind performance, boundary layer wind tunnel

INTRODUCTION

Bluff body aerodynamics plays a critical role in the determination of the principal response of a high-rise building. Tall buildings can be susceptible to excessive motion during wind events that can cause occupant discomfort and reduce the overall appeal of the structure (Kareem, 1992). Furthermore, these excessive motions can create high base loads, which can increase the cost of the structure. Structural engineers generally opt for optimizing the structural system or increasing modal mass to reduce wind-induced motion, as discussed by Kareem (1983). Building motions can also be mitigated by supplemental damping systems, as explained by Brazil et al. (2006) and Breukelman and Haskett (2001). However, consideration of building shape can also lead to improved wind performance (Irwin 2008, and Irwin et al. 1998). This study looked to identify general wind loading patterns for common building shapes, with the objective of encouraging designers to consider bluff body aerodynamics early in the design process.

Shape effects, from a wind engineering perspective, have been investigated by Davenport (1971), via aerodynamic model tests. Hayashida and Iwasa (1990) also examined shape effects on super tall building using rigid models. Corner modifications and their impact on aerodynamic forces were studied in detail by Dutton and Isyumov (1990), Kawai (1998) and Tamura and Miyagi (1999). The present study looks to expand on and support past research, by examining the wind loading patterns on various shapes on a direction by direction basis. The computed wind loads are also benchmarked against two international building standards, the NBCC 2005 and the ASCE 7-2005.

Zhou et al. (2003) provided a novel approach to give designers the necessary knowledge to effectively design structures for wind performance. The respective authors compiled a database of high-frequency base balance (HFBB) test data for structures of various heights and footprints. By inputting key building parameters, designers are provided with an estimate of the wind response of the structure. Our research is intended to supplement the information presented by Zhou et al. (2003), and demonstrate general wind loading patterns for common building shapes. Zhou et al. (2003) suggested that loading data accumulated via commercial wind tunnels tests of buildings in their actual surroundings could be used to supplement an overall loading database. It is encouraging to see the use of such databases for preliminary design purposes included i the commentaries of ASCE 7-05 such as *http://aerodata.ce.nd.edu/interface/ interface.html*

The present study further strengthens this approach by utilizing aerodynamic model studies for actual buildings using high-frequency force balance (HFFB) method conducted by the RWDI group of companies. The HFFB method is a commonly used technique in determining the wind-induced response of tall building. The method, also referred to as the high-frequency base balance, was originally developed by Tschanz and Davenport (1983), and has been in practice for many years as a cost effective way of measuring wind induced loads. The HFFB methodology includes collecting a time history of the base loads (shear forces, bending moments and torsion) on a scaled aerodynamic model in a boundary layer wind tunnel. The rigid aerodynamic model is mounted on a special six degree-of-freedom load cell to measure the base loads, while the inertial loads are evaluated analytically. The dynamic loads and computed inertial loads are then combined to provide the peak design loads. The basic assumption in HFFB tests is that feedback due to aeroelastic effects (i.e. building motions) is negligible compared to the aerodynamic and inertial forces. As such, reasonable wind-induced responses can be obtained by testing a rigid model in a boundary layer wind tunnel. The scaled aerodynamic model, while replicating the shape of the study building, should be light and rigid to avoid any resonance effects due to model vibration and have a flat spectral response due to high damping. For the present study, aerodynamic models with a resonant frequency in the order of approximately 100 Hz were used. While the time histories of the base loads are scaled appropriately to provide the mean and background loads for the test building at full scale, the resonant components are obtained analytically by solving the equation of motion (Tschanz and Davenport (1983), Boggs and Peterka (1989), Xie and Irwin (1998)). The equation of motion governing the fundamental mode of vibration of a tall structure using generalized coordinates is given by Eq. (1),

$$m^*\ddot{x} + c^*\dot{x} + k^*x = P \;\; m^*\ddot{x} + c^*\dot{x} + k^*x = P \tag{1}$$

where m^* m^* c^* c^* k^*, P and x are the generalized mass, damping, stiffness, load, and response, respectively. These parameters are functions of the structure's mass distribution, m m, mode shape, f, natural frequency, f_o f_o, externally applied load, P, displacement of the structure, x and critical damping ratio, ζ. For a lumped-mass system, these parameters take the following form:

$$m^* = \{f\}^T [m]\{f\}$$
$$k^* = (2\pi f_o)^2 m^*$$
$$c^* = 2\zeta\sqrt{m^* k^*}$$
$$P^*(t) = \{f\}^T \{P\} = \sum P_i f_i$$
$$\{x\} = x(t)\{f\}$$

For buildings having linear mode shapes (i.e. $f_i = z/H$ $f_i = z/H$) the generalized force, which is the right hand side RHS of Eq. (1), is the same as the moment at the base, as shown in Eq. (2),

$$\sum P_i f_i = \frac{1}{H}\sum P_i z_i = \frac{M}{H}\sum P_i f_i = \frac{1}{H}\sum P_i z_i = \frac{M}{H} \tag{2}$$

where H and M are the height and base moment of the building, respectively. Since the wind induced generalized force is known via wind tunnel testing, we can use the structural dynamic properties of the full scale building and assumed damping ratios to solve for the unknowns on the left hand side of Eq. (1). This process is usually carried out in the frequency domain. The power spectral density, $S_{p*}(f)\,S_{p*}(f)$, for the base moment is computed first using Eq. (3). The generalized response load for each mode can be obtained by integrating the area under the spectral density function (Eq. 3), as shown in Eq. (4). The contributions from each mode will be combined by using square root of the sum of the squares (SRSS) method to obtain the total generalized response $s_T^2 s_T^2$. $S(f)S(f)$ represents the mean square spectral density, commonly referred to as the power spectral density (PSD).

$$S_x = \frac{1}{k^{*2}} |\mathrm{H}(f)|^2 \, S_{p*}(f) S_x = \frac{1}{k^{*2}} |\mathrm{H}(f)|^2 \, S_{p*}(f) \tag{3}$$

$$H(f)|^2 = \frac{1}{\left[1 - \left(\frac{f}{f_0}\right)^2\right]^2 + \left(\frac{2zf}{f_0}\right)^2}$$

$$s_x = \frac{1}{k^*}\left(\int_0^\infty |H(f)|^2 \, S_{p*}(f)\,df\right)^{1/2} \quad s_x = \frac{1}{k^*}\left(\int_0^\infty |H(f)|^2 \, S_{p*}(f)\,df\right)^{1/2} \tag{4}$$

The difference between the square of generalized response load, $s_T^2 s_T^2$, and the square of the background load, $s_B^2 s_B^2$, represents the resonant loading contributions. Note that $s_B^2 s_B^2$ can be obtained by integrating the spectral density function, $S_{p*}(f)\,S_{p*}(f)$, of the base moment time history. More details on HFFB background, along with corrections for non-ideal mode shapes and approximate load distribution over the height of the building, can be found in Boggs and Peterka (1989), Xie and Irwin (1998), Chen and Kareem (2005a), and Chen and Kareem (2005b). It is worthy of note that the structural properties of a study building are used only during the analytical procedure. Thus the HFFB wind tunnel data can be re-analyzed for new set of revised structural properties, as required, to generate a new set of wind responses provided that the shape of the building remains similar.

Hundreds of HFFB studies were considered for inclusion in this study. The intent was to show general wind load patterns for various building shapes. Availability of this type of information is believed to aid designers in assessing wind responses at the early design stages. Seed buildings were selected to have simplistic footprints similar to one of the following five shapes: square, circle, triangle, rectangle and ellipse. The test data from each of the sample seeds were modified to account for geometry differences. The modified test data, now matching a common building geometry, were then combined with an assumed set of dynamic properties to determine the wind response. The results allow for comparisons of the general wind loading patterns of the studied shapes.

SHAPE SELECTION

Common building shapes were selected for inclusion in this study. Figure 1 presents a photo of a seed building for each the shapes studied. Sample seeds were sought to have open surroundings to avoid unique project specific wind effects caused by adjacent structures. From the database, four buildings for each of the five basic building footprints considered were identified. Details of the sample seeds, including shape, width, height, aspect ratio and slenderness ratio, are presented in Appendix A (dimensions shown in full scale meters). The study also considered seeds for various Reynold's numbers (Re), which should be acknowledged when considering the results. The variation of Re for the various experiments was limited to ±150,000.

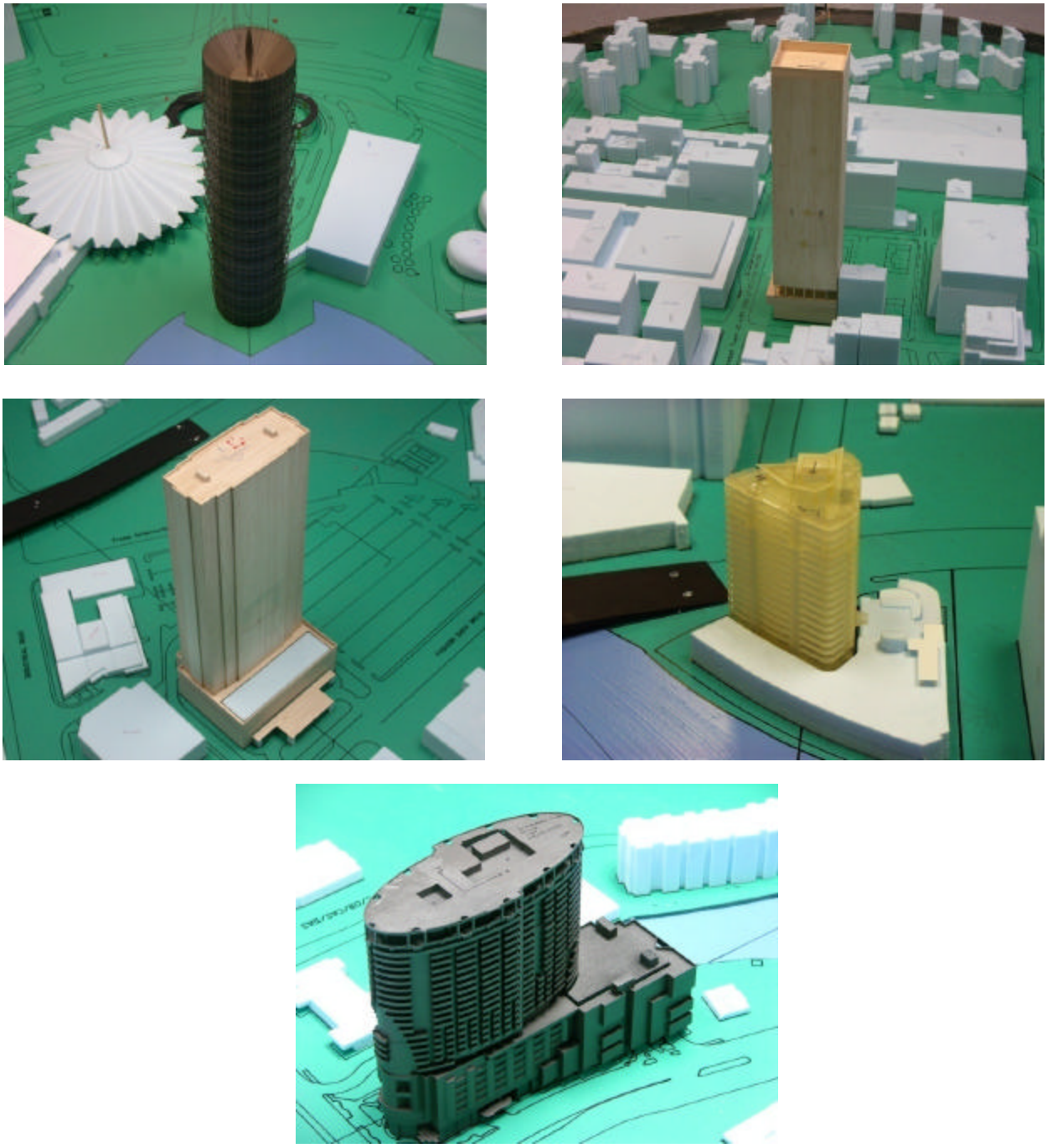

Figure 1. Photos of representative seed buildings.

DATA PROCESSING

Twenty seed buildings were identified for consideration in this research, with four seeds for each of the five study shapes. While the cross-section of each of the seed buildings was similar to one of the five study shapes, the height and width of the seed was varied. In order to compare the data and identify loading trends for particular shapes, it was necessary to normalize the data to represent a common building shape, termed in this paper as representative cylinder. The methodology used to normalize and compute the base loads is discussed in this chapter, while the building and analysis parameters (including the dimensions of the representative cylinders) is discussed in the next section.

The wind loading data from the seed buildings are used to compute the wind loads on the representative cylinders. The data are first reduced into force or moment coefficients using the building shape and test wind speed, and the geometry of the representative cylinder is combined with the moment coefficients to produce the loading on the representative cylinders. The process was repeated for each of the seed buildings, resulting in a set of wind loads that could be compared for each study shape. Eqs. (5) through (9) show the geometric correction factors that were used to convert the seed building loads to be applicable to the geom etry of the representative cylinder.

$$C_{Fx} = \frac{B_{r,x}.h_r.q_{ref}}{B_{s,x}.h_s.q_{ref}} \tag{5}$$

$$C_{Fy} = \frac{B_{r,y}.h_r.q_{ref}}{B_{s,y}.h_s.q_{ref}} \tag{6}$$

$$C_{My} = \frac{B_{r,x}.h_r^{\,2}.q_{ref}}{B_{s,x}.h_s^{\,2}.q_{ref}} \tag{7}$$

$$C_{Mx} = \frac{B_{r,y}.h_r^{\,2}.q_{ref}}{B_{s,y}.h_s^{\,2}.q_{ref}} \tag{8}$$

$$C_{Mz} = \frac{\left(B_{r,x}^{\,2} + B_{r,y}^{\,2}\right).h_R.q_{ref}}{\left(B_{s,x}^{\,2} + B_{s,y}^{\,2}\right).h_R.q_{ref}} \tag{9}$$

In Eqs. (5) through (9), h is the building height; B is the effective width normal to the X or Y axis as indicated; the subscripts s and r denote the seed building and representative cylinder, respectively; and, q_{ref} is the mean velocity pressure at a reference height, taken to be 1.5 m above the floor of the BLWT for all tests (i.e. 600 m at full-scale). These geometric correction factors were applied to the model scale measurements from the BLWT test of each of the seed buildings. The RMS of the base forces and moments for the representative cylinders were computed using the following equation

$$s_{r,i} = s_{s,i} \times C_i$$

where s is the RMS response; C_i is the geometric correction factor for load *i*; the subscript *i* denotes one of $F_xF_x, F_yF_y, M_yM_y, M_xM_x$ or M_zM_z, the subscripts s and r denote the seed building and representative cylinder, respectively. The seed building data was reduced to obtain the non-dimensional PSD in the following form

$$S_{r,i} = \frac{\left(f \times S_{s,i}(f)\right)}{\left(s_{s,i}\right)^2}$$

where *S* is the PSD; and f is the building frequency. The mean and background wind loads on the representative cylinders are computed using the following

$$\overline{R}_{r,i} = \overline{R}_{s,i} \times C_i$$

$$\overline{R}_{r,i} = g_B \times s_{r,i}$$

where, $\tilde{R}\tilde{R}$ and $\hat{R}\hat{R}$ represent the mean, background and resonant wind response. $g_B g_B$ is the background peak factor, typically around 3.5. The resonant wind loads on the representative cylinders were calculated as follows

$$\hat{R}_{r,i} = g_R \times s_{r,i} \times \sqrt{\frac{p \times S_{r,i}(f_1)}{4z_1}}$$

$$g_R = \sqrt{2\ell n(f_1 T)} + \frac{0.5772}{\sqrt{2\ell n(f_1 T)}}$$

where $g_R g_R$ is the resonant peak factor (Tschanz and Davenport, 1983); T is the observation time $f_1 f_1$ is the natural frequency; and, $z_1 z_1$ is critical damping ratio. The peak response of the building, $\hat{R}\hat{R}$, can then be determined by summing the mean loading with the root of the sum of the squares (SRSS) of the background and resonant components, as shown in Eq. (10).

$$\hat{R} = \overline{R} + \sqrt{\tilde{R}^2 + \hat{R}^2}\,\hat{R} = \overline{R} + \sqrt{\tilde{R}^2 + \hat{R}^2} \tag{10}$$

Following this methodology, the resulting wind loads, derived from the seed buildings, correspond to a common geometry and can be compared on a direction by direction basis to identify general wind loads trends on common building shapes.

EXPERIMENT PARAMETERS

The cross-section of each of the seed buildings matched one of the five study shapes, however, the height and width of the seed was varied. The previous section outlined the methodology to normalize the wind loading data collected from the seed buildings to correspond to a representative cylinder of nominal dimensions. The full scale dimensions and coordinate origins for each of the representative cylinders are shown in Figure 2. The height of the representative cylinders were taken to be 150 m at full scale.

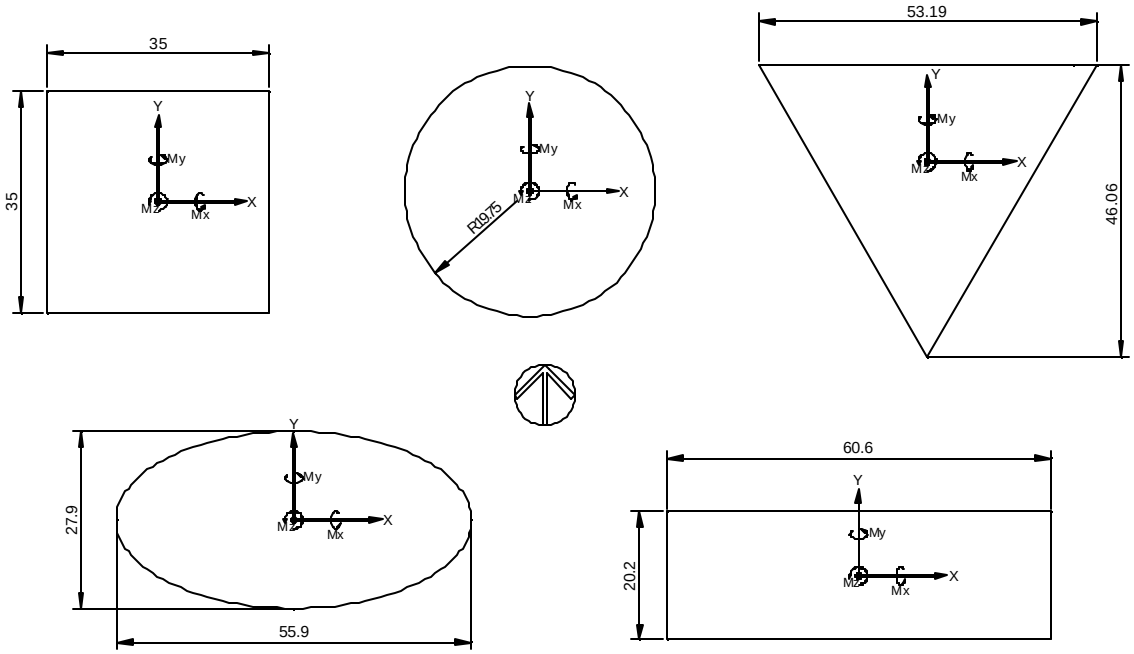

Figure 2. Definition of representative cylinders shapes.

The dimensions shown in Figure 2 were chosen to minimize the geometric correction factors and provide the same cross-sectional area for each representative cylinder. The base overturning moments about *X* and *Y* axis are denoted as M_X and M_Y, respectively. The corresponding base shears along the X and Y axes are denoted throughout this paper as F_x and F_y. The base torsional moment is termed as M_z. The north arrow, in the center of Figure 2, can be used to identify the wind direction. Wind direction is defined as the direction from which the wind blows (commonly referred to as the angle of attack), measured clockwise from north, with north corresponding to 360 degrees.

Assumptions of dynamic properties for the representative cylinders were necessary to permit the computation of the base loads. A building density of 320 kg/m^3 (20 lb/ft^3) was assumed, along with a damping ratio of 2% of critical, which was considered reasonable for strength design of a high-rise structure (Newmark and Hall, 1982). The radius of gyration (R_g) of the structure was estimated as one-third of the diagonal dimension of the representative cylinder. The mass moment of inertia (*MMI*) was then approximated using Eq. (11).

$$MMI = R_g^{\,2} \cdot m \tag{11}$$

In Eq. (11), m indicates the assumed story mass of the representative cylinder. The fundamental natural sway frequencies of the representative structure were approximated based on the height of the building. Table 1 lists the frequencies used in the analysis procedure. For simplicity, only first-order sway and torsion modes were considered. All the three modes were assumed to be linear.

Table 1. Assumed building frequencies.

Cylinder	**Frequency (Hz)**		
	X	Y	Torsion
Square	0.2	0.2	0.4
Circular	0.2	0.2	0.4
Triangular	0.2	0.2	0.4
Rectangular	0.3	0.2	0.4
Elliptical	0.3	0.2	0.4

It should be noted that the present study only looked at a particular configuration of dynamic building properties, as the emphasis was on shape effects. Mass, stiffness and damping levels will no doubt have a significant impact on the loading patterns observed. The effect of these parameters on the general loading patterns of the shapes is discussed in Chan et al. (2009). The impact of mass, stiffness and damping on shape effects is an area that could be examined in future studies in more detail.

The basic design wind speed for the analysis was assumed to be 144 km/hr for 3-second gust at 10 m above ground in open terrain condition. Using the Durst curve for averaging time conversion and the power law for the mean wind speed profile (see Eq. 12), a mean hourly gradient wind speed of 168.5 km/h was calculated.Gradient height was assumed to be 600 m above ground for this investigation.

$$U_g = U_h \cdot \left[\frac{z_g}{z_h} \right]^{0.14} \tag{12}$$

In Eq. (12), *U* and *z* denotes the wind velocity and height above ground, respectively, and the subscripts g and *h* represent gradient height and height of interest, respectively. An open terrain profile, assumed by the exponent in Eq. (12), was used to compute the gradient wind speed. The wind tunnel terrain profile for each of the sample seeds was accounted for via a gust speed correction factor. The wind response of the sample seeds was factored by the ratio of the gust wind speed at the stagnation point during testing of the seeds versus the desired gust speed in an open profile at the stagnation point of the representative cylinder. The resulting factored response gives the wind loading on the representative cylinders.

Wind directionality effects were not considered in this study. Numerous approaches to apply wind direction reductions have been suggested in the literature, but no consensus has been reached (Simiu & Miyata, 2006). Therefore, the results presented in the following sections are the raw base loads and do not account for the probability of extreme winds occurring in each sector.

RESULTS AND DISCUSSION

The wind responses for each of the representative cylinders were derived from the measured seed building data using the methodology and parameters outlined in previous sections. This section presents azimuthal plots of the computed base loads, and indentifies general loading patterns for each of the shapes.

The calculated base loads, on a direction-by direction basis, demonstrate good agreement between the sample seeds. Yet, some variation was observed, which can be expected as the loading data for each of the seeds was retrieved from a distinct wind tunnel test with unique surrounding structures. The authors emphasize that they are in no way recommending the procedure outlined in this paper as a surrogate for wind tunnel testing. It is only hoped that the findings of this research will encourage designers to consider wind performance early in the design process (when the building shape is contrived). Once the design has reached a mature stage, a BLWT study will still be advisable to determine the specific wind response of the structure.

Figure 3 plots the base sway loads for the square cylinder using the factored data for all four seed buildings. Since all of the sample seeds were factored to match the same geometry, they are not distinctly identified in Figure 3. Rather, the peak dynamic loads for each seed are shown by the blue lines and mean loading is identified by the red series. The average of the four seeds is shown with a thick black line, with the uppermost line being the maximum, the lowermost line being the minimum, and the middle line showing the mean wind loading. As a benchmark, the ASCE 7-05 (cyan) and the NBCC 2005 (pink) peak base loads are also included in the plot.

From the sway moment and shear plots in Figure 3, peak lift moments are evident from 180 and 360 for M_y and $S_{x,}$ and from 90^0 and 270^0 for the M_x and S_y loading. These peak loads are caused by vortex shedding, which is identified by the signature high dynamic spikes and zero mean-loading values. The code calculated wind loads from the ASCE 7-05 and NBCC 2005 demonstrate good agreement when estimating the drag moments and shears, but fail to forecast the peak lift loads. Building designers should be aware of this occurrence and investigate methods to remedy the problem, or employ wind testing techniques to quantify the lift loading. The mitigation technique of corner modification was used by Irwin (2008) for the Taipei 101 Tower, and a 25% reduction on the base sway moments was reported. Browne et al. (2005) also discusses the efficiency of balconies located at corners in disrupting the formation of coherent vortices, which is the main source of liftforces.

Figure 4 illustrates the base loads for each wind direction as experienced by the circular cylinder. Again, the computed wind loads from the ASCE 7-05 (cyan) and the 2005 NBCC (pink) are shown.

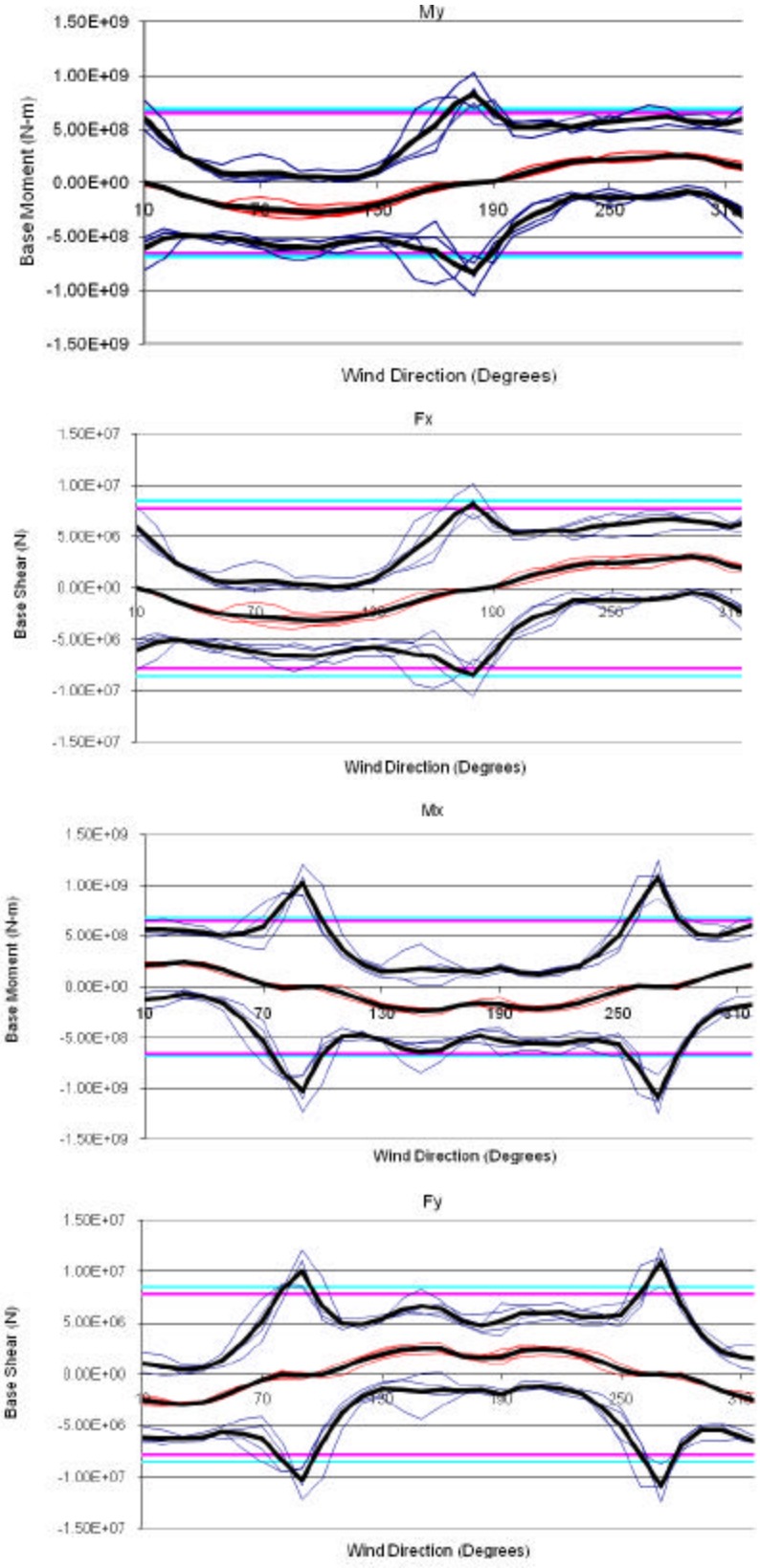

Figure 3. Base moments and shears for square cylinder.

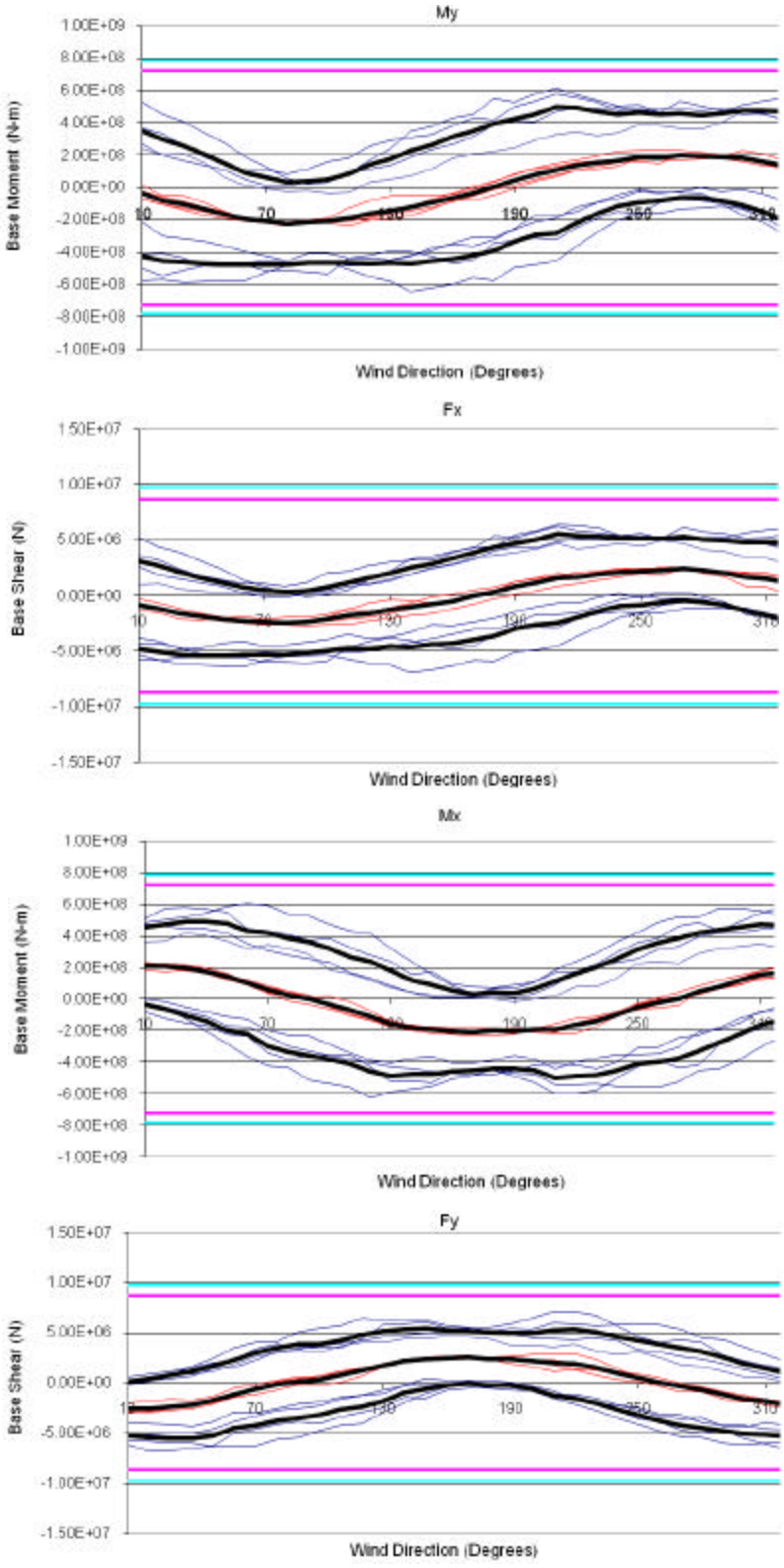

Figure 4. Base moments and shears for circular cylinder.

The code prescribed loads are sufficient in estimating the peak dynamic loads on the circular cylinder, with all of the seeds contained by the estimates. Vortex shedding was not distinctly observed. This was attributed to the fact the sample seeds were generally large radius, rough-walled cylinders capable of producing super-critical Reynolds number flow in the BLWT. For smooth cylindrical structures of smaller radii, such as air traffic control towers or chimney stacks, vortex-induced oscillation may be prevalent as suggested by Jackson (1987) and Simiu and Scanlan (1996).

The base loads of the factored sample seeds for the representative triangular cylinder are provided in Figure 5.

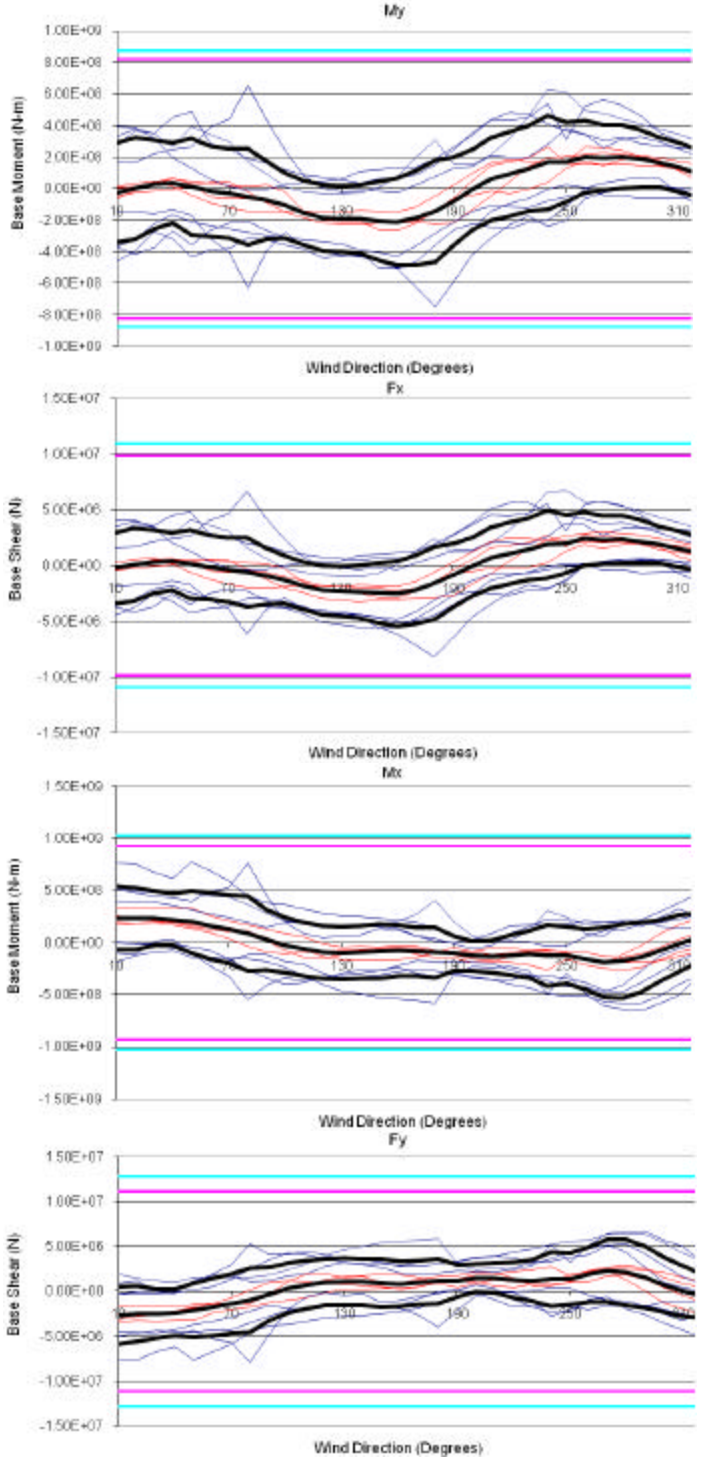

Figure 5. Base moments and shears for triangular cylinder.

All of the computed base loads on the triangular cylinder are less than those computed by building code. This is due to the fact that the code calculation is based on the projected width of the cylinder and does not account for the aerodynamics of the shape. Note that even from wind directions normal to a face of the triangular section, the wind loads are significantly less than the anticipated building code value. Consequently, savings in terms of cost and materials may be available resulting from the application of wind tunnel testing methods versus code provisions for the design of triangular structures. It would also be interesting to investigate the resultant base loads that occur simultaneously on the triangular cylinder, since Figure 5 shows coupling between the X and Y direction forces for wind direction 260 .

Figure 6 depicts the calculated loads at the base of the rectangular cylinder, along with the load estimates derived from the building codes.

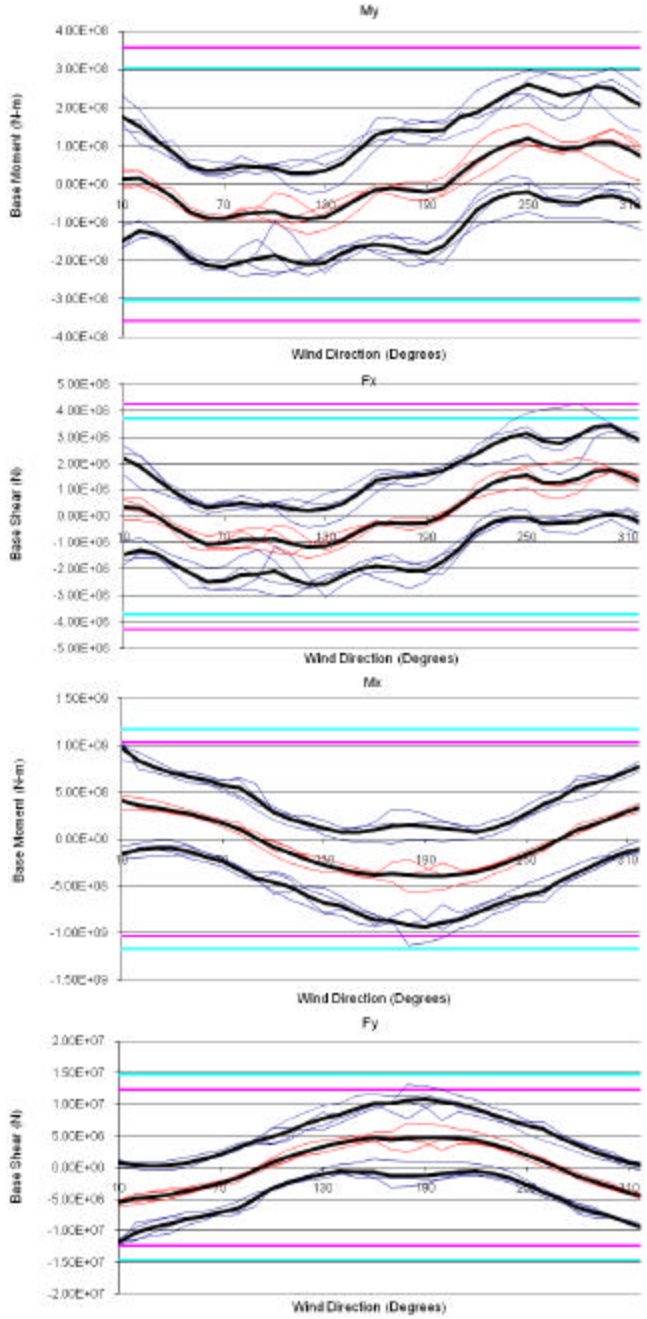

Figure 6. Base moments and shears for rectangular cylinder.

Although a rectangular cylinder closely resembles a square cylinder in shape, the azimuthal force plots for the rectangular section shown in Figure 6 are drastically different from those presented in Figure 3 for a square section. Peak dynamic lift moments caused by vortex shedding, which were evident on the square cylinder were not present in the results for the rectangular cylinder. Furthermore, the code provisions did an excellent job predicting the base wind loads.

The base loads calculated from the factored wind tunnel response of the elliptical seeds can be seen in Figure 7.

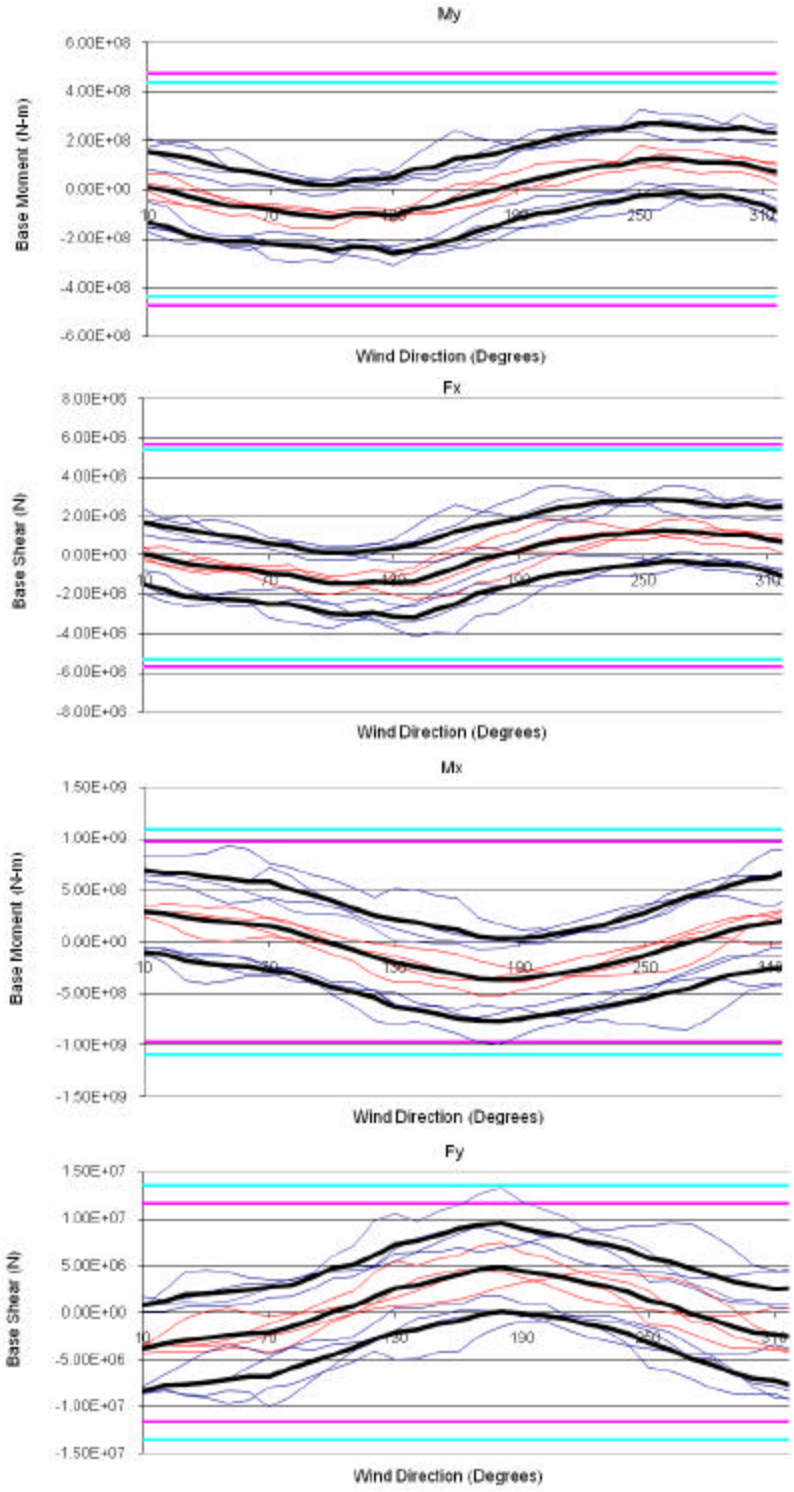

Figure 7. Base moments and shears for elliptical cylinder.

Figure 7 illustrates that the wind loads experienced by the elliptical cylinder in the X-direction (F_x, M_y) are significantly less than the code wind loads. The drag coefficient for an ellipse in the X-direction gives an indication that the wind load experienced by the elliptical cylinder will be considerably less than that calculated for a rectangle. Since the code provisions assume a rectangular section, it seems logical that the X-direction loads on an ellipse would be less than the code predictions. Again, this presents an opportunity for savings through the utilization of BLWT testing. The Y-direction loads (F_y, M_x) fall in line with the code values. High dynamic loads caused by vortex induced oscillation were not apparent in any of the plots in Figure 7.

For design conditions where torsional loads are critical, the torsional eccentricity gives an indication as to how effective a building shape is in reducing torsional loading. The torsion eccentricity is a function of the torsional moment, M_z, the peak base shear, S, and the maximum projected building width, with the relationship shown as Eq. (13).

$$e = \frac{M_z}{\hat{S} \cdot \hat{B}} \tag{13}$$

The torsional eccentricity was calculated for all sample seeds and averaged across each study shape. The average torsion offset for each of the researched shapes is presented in Table 2.

Table 2. Torsional eccentricity for study shapes.

Shape	Torsional Eccentricity
Square	8.3%
Circle	4.0%
Triangle	15.4%
Rectangle	11.4%
Ellipse	10.7%

Table 2 clearly shows that the circular buildings are very effective at reducing torsional loads. Of course, a truly circular building cannot develop any torsional loading about its central axis. Any torsional loads measured on a circular building would be the result of asymmetric surrounding buildings or dynamic loads due to an offset center of mass. Since the center of mass was fixed at the geometric center for this study, the observed torsional loads can be attributed to the presence of unique surrounding buildings adjacent to each of the sample seeds, which produced nominal torsional excitation.

The square seed buildings generated a torsion offset two times greater than that of the circular cylinder. Greater still are the torsion loads generated by the elliptical and rectangular sections, which was to be expected given the wider building dimension in the projected Y-direction. Thus, if reducing torsion loads or torsional velocities is critical for the design of structure, using a circular or square footprint over a elliptical or rectangular floor plan would be advised. Finally, Table 2 shows the high torsion offset present in the triangular section. The torsion offset for the triangular shape exceeded that of all other studied shapes, making the triangular section a poor choice for torsion-sensitive structures.

CONCLUSIONS

The results described above outline the general wind loading characteristics of simplistic building shapes. The data indicate certain shapes that are prone to wind phenomena, such as vortex-shedding, which can generate high dynamic loads and govern the design. Elliptical, triangular and rectangular shaped buildings were identified as being more susceptible to high torsion loading. While the methods presented in the paper are not intended for the determination of design wind loads, it is believed that the general wind loading

patterns illustrated by the authors will be useful in building design circles. It is hoped that this modest research will ignite an interest on the use of aerodynamic shapes and the consideration of building shape, in terms of wind performance, early in the design process.

The intention of the current paper was to focus on shape effects. However, future research could include exploring the sensitivity of each shape to the dynamic properties of the structure (i.e. mass, stiffness, damping). Furthermore, the study could be expanded to include other shapes, such as L-shaped and Y-shaped buildings, buildings with chamfered corners or structures with particular aspect ratios.

ACKNOWLEDGEMENTS

The authors would gratefully acknowledge RWDI group of companies for access to their extensive database of BLWT test data.

REFERENCES

1. American Society of Civil Engineers. 2005. "ASCE 7-05 Standard Minimum Design Loads for Buildings and Other Structures". Reston, Virginia.
2. Boggs, D.W., and J.A. Peterka. 1989. "Aerodynamic model tests of tall buildings". Journal of Engineering Mechanics. 115 (3), 618-635.
3. Brazil, A., L.M. Joseph, D. Poon, and T. Scarangelo. 2006. "Designing High Rises for Wind Performance". ASCE: Structures Congress 2006.
4. Breukelman, B, and Haskett, T. (2001). "Good Vibrations". Civil Engineering. ASCE: Dec. 2001.
5. Browne, M. Suresh Kumar, K. 2005. "Effect of Corner Balconies on Wind-Induced Response of Tall Buildings". The 10th Americas Conference on Wind Engineering. Baton Rouge, Louisiana.
6. Chan C.M., J.K.L Chu, and M.F. Huang. 2009. "Integrated Aerodynamic Load Determination and Stiffness Design Optimization of Tall Buildings". Structural Design of Tall and Special Buildings. 18, 59-80.
7. Chen, X., and A. Kareem. (2005a). "Validity of Wind Load Distribution based on High Frequency Force Balance Measurements". Journal of Structural Engineering. June 2005, 984-987.
8. Chen, X., and A. Kareem. (2005b). "Dynamic Wind Effects of Buildings with 3D Coupled Modes: Application on High Frequency Force Balance Measurements". Journal of Engineering Mechanics. November 2005, 1115-1125.
9. Davenport, A.G. 1971. "The Response of Six Building Shapes to Turbulent Wind". Philosophical Transactions of the Royal Society of London. 269 (1199), 385-394.
10. Dutton, R., and N. Isyumov. 1990. "Reduction of Tall Building Motion by Aerodynamic Treatments". Journal of Wind Engineering and Industrial Aerodynamics. 36, 739-747.
11. Hayashida, H., and Y. Iwasa. 1990. "Aerodynamic Shape Effects of Tall Building for Vortex Induced Vibration". Journal of Wind Engineering and Industrial Aerodynamics. 33, 237-242.
12. Irwin, P.A. 2008. "Bluff Body Aerodynamics in Wind Engineering". Journal of Wind Engineering and Industrial Aerodynamics. 96, 701-712.
13. Irwin, P., B. Breukelman, C. Williams, and M. Hunter. 1998. "Shaping and Orienting Tall Buildings for Wind". 1st World Structures Congress, San Francisco, CA.
14. Jackson, C.P. 1987. "A Finite-Element Study of the Onset of Vortex Shedding in Flow Past Variously Shaped Bodies". Journal of Fluid Mechanics. 182, 23-45.
15. Kareem, A. 1992. "Dynamic Response of High-Rise Buildings to Stochastic Wind Loads". Journal of Wind Engineering and Industrial Aerodynamics. 41-44, 1101-1112.
16. Kareem, A. 1983. "Mitigation of Wind Induced Motion of Tall Buildings". Journal of Wind Engineering and Industrial Aerodynamics. 11, 273-284.
17. Kawai, H. 1998. "Effect of Corner Modifications on Aeroelastic Instabilities of Tall Buildings". Journal of Wind Engineering and Industrial Aerodynamics. 74-76, 719-729.

18. National Research Council of Canada - Institute of Research in Construction. 2005. "National Building Code of Canada". Ottawa, Ontario.
19. Newmark, N., and W. Hall. 1982. "Earthquake Spectra and Design". Earthquake Engineering and Research Institute.
20. Merrick, R. and G. Bitsuamlak, G.T. (2008) "Control of flow around a circular cylinder by the use of surface roughness: A computational and experimental approach", 4th International Conference on Advances in Wind and Structures (AWAS08), May 2008, Jeju, Korea.
21. Simiu, E., and T. Miyata. 2006. "Design of Buildings and Bridges for Wind". John Wiley & Sons, New Jersey. Simiu, E., and R. Scanlan. 1996. "Wind Effects on Structures". John Wiley & Sons, New York.
22. Tamura, T., and T. Miyagi. 1999. "The Effect of Turbulence on Aerodynamic Forces on a Square Cylinder with Various Corner Shapes". Journal of Wind Engineering and Industrial Aerodynamics. 83, 135-145.
23. Tschanz, T., and A. G. Davenport. 1983. "The Base Balance Technique for the Determination of DynamicWind Loads". Journal of Wind Engineering and Industrial Aerodynamics. 13, 429-439.
24. Xie, J., and P.A. Irwin. 1998. "Application of Force Balance Technique to a Building Complex". Journal of Wind Engineering and Industrial Aerodynamics. 77&78, 579-590.
25. Zhou, Y., T. Kijewski, and A. Kareem. 2003. "Aerodynamic Loads on Tall Buildings: Interactive Data base". Journal of Structural Engineering. ASCE: March 2006, 394-404.

APPENDIX A. Seed Building Information.

Footprint	Height (m)	Max. Width (m)	Aspect Ratio	Slenderness Ratio
	242	34	1.02	7.26
	264	34	1.00	7.76
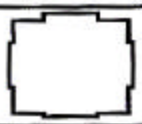	278	35	1.00	7.94
	148	29	1.18	6.02
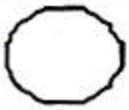	262	58	1.00	4.52
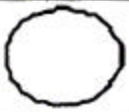	102	13	1.00	7.85
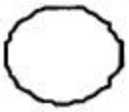	156	40	1.00	3.90
	96	10	1.00	9.60
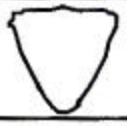	350	56	1.20	7.50
	235	60	1.08	4.23

APPENDIX A. Seed Building Information (cont'd).

Footprint	Height (m)	Max. Width (m)	Aspect Ratio	Slenderness Ratio
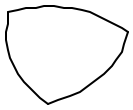	174	45	1.05	4.06
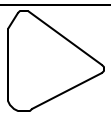	67	35	1.23	2.35
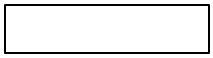	98	77	3.35	4.26
	121	67	2.23	4.02
	193	82	2.33	5.48
	100	41	1.83	4.46
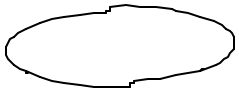	107	100	2.37	2.54
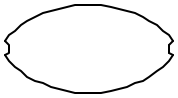	96	48	1.53	3.06
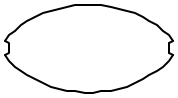	96	48	1.53	3.06
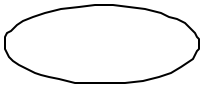	120	49	1.99	4.87

Journal of Wind and Engineering, Vol. 6, No. 2, July 2009, pp. 19-29

SIMULATION STUDIES ON DESIGN OF VORTEX GENERATORS FOR BOUNDARY LAYER WIND TUNNEL

S. Selvi Rajan[1], N. Lakshmanan[2], S. Arunachalam[3], G. Ramesh Babu[1]
Structural Engineering Research Centre, Chennai, India
sselvi@sercm.org

[1] Scientist , [2] Project Advisor, [3] Director Grade Scientist, Advisor (management)

ABSTRACT

Studies on wind tunnel require proper stimulation of atmospheric boundary layer wind characteristics, which is random both in time and space. The present study focuses simulation of atmospheric boundary layer using Wind Tunnel test facility of SERC Chennai. The development of velocity profile along the length of the test section has been studied for evaluating the stability criteria for atmospheric boundary layer flows. Equations have also been derived for evaluating the region beyond which such stability has been realised for various combinations of trip board height andheight of roughness elements. Analytical and empirical equations to obtain the important characteristics of wind flow in the atmospheric boundary layer namely power law coefficient, aerodynamic roughness length, thickness of boundary layer, momentum thickness, displacement thickness and shape factor have been derived. The inter-relationships among these parameters have also been studied and validated. The boundary layer parameters have been further compared with the values reported in literature.

Key Words: Boundary Layer Wind Tunnel, Simulation, Power law coefficient, Spectrum

INTRODUCTION

One of the main requirements in the simulation of atmospheric boundary layer in a wind tunnel is that the models should be adequately immersed within the thickness of developed boundary layer. However the space and construction constraints have led to the use of short test section lengths in most of the wind tunnels. Further, evolution of boundary layer wind tunnels from the modification of the conventional aeronautical wind tunnels generally had lesser test section lengths, while their widths were sufficiently large of the order of 3 to 4 m [Cermak, 1982]. Hence the use of various vortex generators such as spires, trip board / fence, barrier, saw-tooth devices, etc., along with floor roughening elements came into existence in order to achieve the required development of atmospheric boundary layer in the wind tunnel [Irwin, 1981; Cermak & Cochran, 1992; Sivaramakrishnan & Brij Mohan, 1992; Noda et al, 1995; Cook, 1985 and Reinhold, 1982].

Several combinations of the above mentioned vortex-generation or flow-thickening devices are being used by various investigators for their wind tunnel studies. For example, the use of Standen spires along with floor roughening elements is a much popular system in North America [Cermak & Cochran, 1992]. Use of Counihan spires, castellated barrier, grid and roughness elements is popular in Europe [Counihan, 1970; Hansen & Sorensen, 1985]. Combination of trip board or barrier and roughening elements is popular in Australia [Holmes & Osnosphasop, 1983]. The latter system is claimed to be simple in nature, while it enables achievement of the required boundary layer growth in the wind tunnel [Holmes & Osnosphasop, 1983]. It may be noted that performance of a particular combination of vortex generators for a given wind tunnel depends on the aerodynamic characteristics of the wind tunnel itself. Irwin [1981] suggested some

empirical formulae for dimensioning of the spires with roughness elements - vortex generation system for simulating atmospheric boundary layer corresponding to different power law coefficients. On similar lines, Holmes [1983] reported that use of trip board along with roughening elements system required a fetch length of about 30 to 40 times the trip board height for achieving the equilibrium boundary layer in the tunnel. In the present paper, details of a systematic investigation on simulation of atmospheric boundary layer in wind tunnel at SERC Chennai (Fig. 1), using combination of trip board and roughness elements are presented.

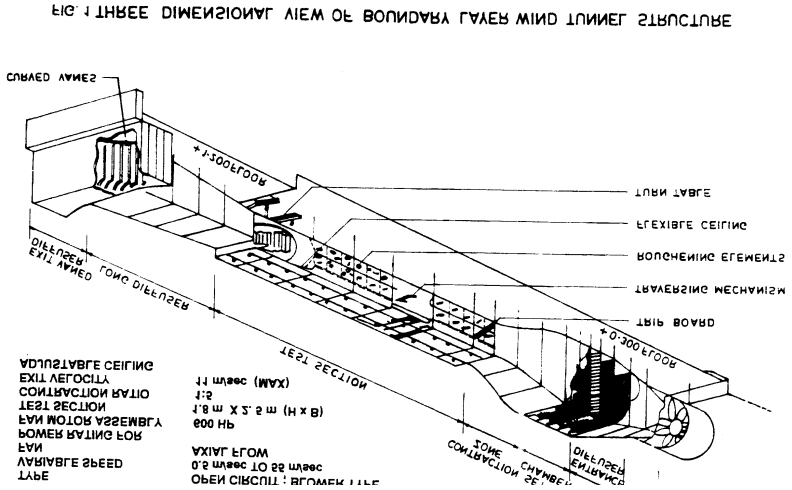

Fig. 1: Three Dimensional View of BLWT Structure

TEST PROGRAMME

Tests were conducted to study the turbulent characteristics of the boundary layer by varying the height of trip board and changing the sizes of the roughening elements. For the present study, the following arrangements were used:

1. 20 cm trip board followed by 5 sheets of roughening cubes of size 4.3 cm x 4.3 cm x 4.3 cm in the upstream and 2 sheets of roughening elements of size 10 cm x 8 cm x 4.3 cm in the downstream, as shown in Fig. 2.
2. 30 cm height trip board followed by the same set of sheets of roughening cubes mentioned in (1).
3. 35 cm height trip board followed by the same set of sheets of roughening cubes mentioned in (1).
4. The 2 sheets of roughening elements of bigger size in the down-stream end as mentioned in (1) were replaced with smaller size cubes of 4.3 cm x 4.3 cm x 4.3 cm, thus having uniform roughening elements all along the test section. Besides roughness cubes, tripping board of 20 cm height is also placed near the entrance of the upstream section.
5. With the same roughness cubes as mentioned in (4), the height of the trip board is increased to 30 cm.
6. 35 cm height trip board is placed instead of 30 cm followed by the same arrangement of roughening elements as mentioned in (4).
7. Only evenly spaced roughening elements with no trip board.

Wind traces were measured using a single probe hot wire anemometer having 1 kHz sampling frequency for 8192 samples. This means that the samples are acquired for a sampling period of more than 8 seconds at one location in the tunnel, which is required to be collected to study the power spectra. However, it is realized that to improve the quality of the results for analysis of spectrum, the sampling frequency and the sampling duration need to be increased further. The acquisition of hot wire signals was carried out using the available software "STREAMLINE". The software is also capable of controlling the movement of traversing system, which enables to measure the velocity variation at different heights. The free-stream velocity of the flow in the wind tunnel was kept approximately at 25 m/sec for all the test programmes. The velocity data were collected at 8 locations along the centre-line of the tunnel in the stream-wise direction at

an interval of about 1.5m to 2 m. The longitudinal fluctuations in the wind velocity were obtained at heights varying from 2 cm to 10 cm intervals above the tunnel floor covering 19 points at each location, accounting to a total number of hot wire anemometer time series data of 684, considering all test cases. 19 points correspond to 2, 3, 4, 5, 6, 7, 8, 9, 10, 20, 30, 40, 50, 60, 70, 80, 90, 100 and 112 cm, measured from the floor of the tunnel.

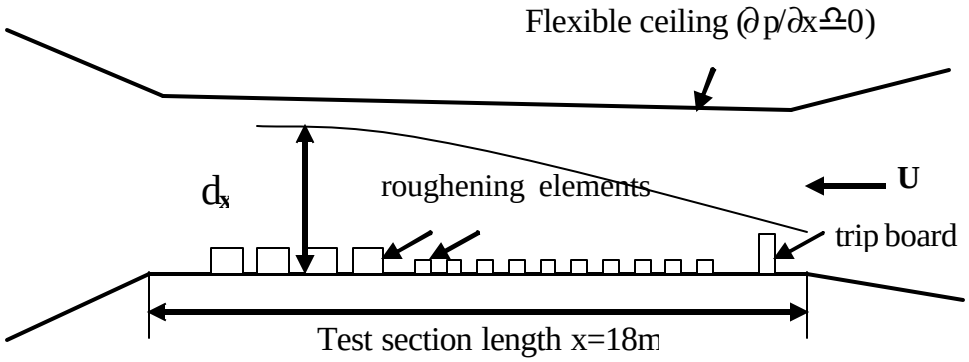

Fig. 2: Long-test-section of the wind tunnel

ANALYSIS OF TEST DATA

Evaluation of Trip Moment

The development of mean velocity profiles along the test section length of the tunnel is shown in Fig. 3, typically for the test case using 30 cm height trip board. The trip moment is defined as a velocity moment caused by the provision of trip board. The values of shear friction velocity u* and aerodynamic roughness length z_0 are evaluated directly from log law model. Assuming power law (being power law coefficient) to be valid for the velocity profiles, it can be shown that the moment at any distance x, M(x), is given by

$$M(x) = \int_0^d U(z) z.dz + \frac{\left(H(x)^2 - d^2\right)}{2}\overline{U} \tag{1}$$

where U(z) is the velocity at any height z, $\overline{U}$ is the free-stream mean velocity, d is the boundary layer thickness and H(x) is the height of the tunnel along the distance x. The total quantity of flow per metre Q is,

$$Q = \left[\int_0^d \left(\frac{z}{d}\right)^a dz + \left(H(x) - d\right)\right]\overline{U} \tag{2}$$

The final moment, M_f can thus be written as:

$$M_f = \int_0^d U(z) z.dz + \left(\frac{H(x)^2 - d^2}{2}\right)\overline{U} - \frac{QH(x)}{2} \tag{3}$$

Substituting Eq.(2) for Q in Eq.(3) and integrating the final trip moment M_f can be evaluated as:

$$M_f = \left[\frac{d^2}{a+2} - \frac{d}{a+1}\frac{H(x)}{2} + \left(\frac{H(x) - d}{2}\right)d\right]\overline{U} \tag{4}$$

When, H(x) $\approx d$ and with a known value of M_f, the value of 'a 'can be directly obtained using equation:

$$\frac{M_f}{\overline{U}} = \frac{d^2.a}{2(a+1)(a+2)} \tag{5}$$

The variation of moment computed along the longitudinal axis of the wind tunnel is shown in Fig. 4. The variation can be adequately represented by the following equations:

$$M(x) = M_f + (M_T - M_f)\,[1.0 - 4.945\,(x/L)^3\,] \quad \text{for } 0 < x < 0.45L \tag{6}$$

and $$M(x) = M_f + 3.3\,(M_T - M_f)\,[1-(x/L)]^3 \quad \text{for } 0.45\,L < x \leq L \tag{7}$$

where M(x) = trip moment at any distance 'x',

M_f = final moment for velocity profile,

M_T = value of trip moment at entry

and L = stabilisation length

Based on Fig.4, the stabilisation length L required is to be around 22 times the trip board height for a smaller trip board of 0.2 m. The above empirical relation is also cross-checked by running the tunnel at a lower velocity.

In majority of the cases tested, the value of d is found to be less than H(x), and hence the expression given in Eq.4 for M_f has to be used. However, as can be seen, there are two unknowns a and d in the above equations for given values of final moment. Based on the experimental studies conducted, the value of d can be taken as 4.0 times the trip board height for 20 cm, 3.5 times the trip board height for 30 cm and 3.0 times the trip board height for 35 cm. Based on all the test cases, an empirical relationship was obtained in terms of not only the trip board size, Tp, but also the size of roughening elements, d, as:

$$a = \left(\frac{0.25T_p + 3d_e}{H_L} \right)^{0.8} \tag{8}$$

where $$d_e = \sqrt{\frac{2(n_1 d_1^2 + n_2 d_2^2)}{N}} \tag{9}$$

n_1 = no.of sheets having an element depth of d_1
n_2 = no.of sheets having an element depth of d_2
H_L = Height of the test section at downstream end
and N = $n_1 + n_2$

Table 1 provides the comparison of a values obtained based on Eq.(8) and experiment for all test cases.

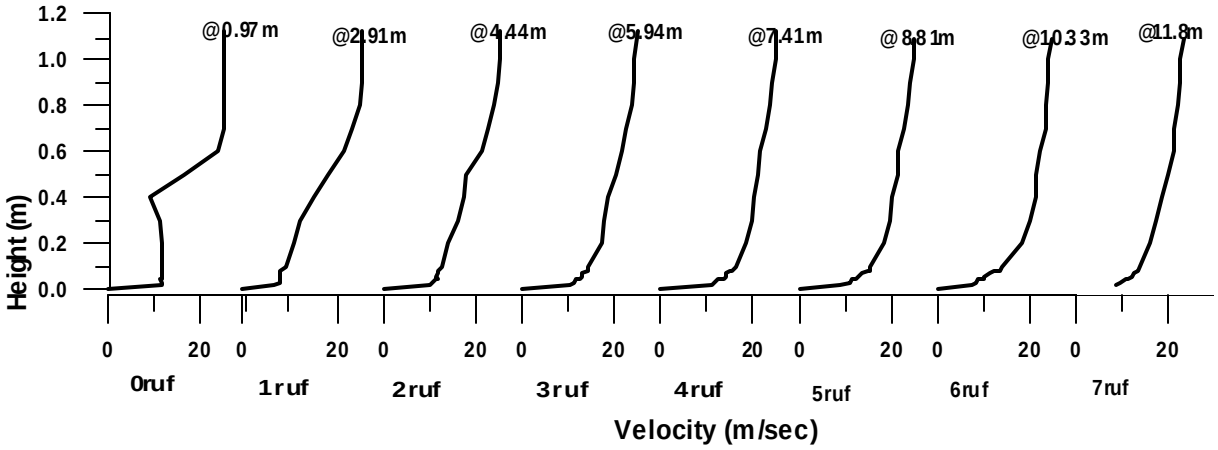

Fig. 3: Mean Velocity Profile along the Test Section for 30 cm Trip Board Case

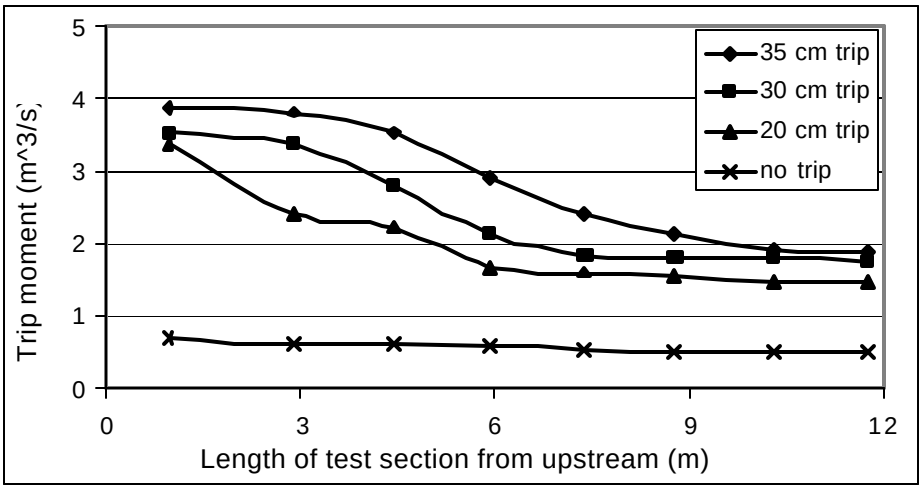

Fig. 4: Variation of Moment along the longitudinal axis of the Wind Tunnel

Table 1: Comparison of experimental values of a with the empirical values

Trip board height (cm)	small and big roughening elements		small roughening elements	
	(expt.)	(theort.)	(expt.)	(theort.)
35	0.25	0.25	0.20	0.21
30	0.24	0.24	0.19	0.20
20	0.20	0.22	0.17	0.18
0	-	0.19	0.16	0.16

Evaluation of displacement thickness

The boundary layer profiles can also be used for the calculation of displacement thickness d^* defined as [Rangaraju et al, 1976]:

$$d^* = \int \left(1 - \frac{\overline{U}(z)}{\overline{U}(d)}\right) dz \tag{10}$$

where $\overline{U}(d)$ = free stream velocity above a boundary layer thickness of
Applying power law,

$$d^* = \int_0^d \left[1 - \left(\frac{z}{d}\right)^a\right] dz = d - \frac{d}{a+1} \tag{11}$$

For z $\geq d$ due to free stream velocity of the atmospheric boundary layer

$$\frac{d^*}{d} = \frac{a}{a+1} \tag{12}$$

Evaluation of momentum thickness

Similar to mass flow rate of boundary layer, d^*, the momentum transport rate of boundary layer, q, is also important in connection with pressure and shear forces [Schlichting, 1980]. The loss of momentum due to boundary layer is given by.

$$q = \int \left(1 - \frac{\overline{U}(z)}{\overline{U}(d)}\right) \frac{\overline{U}(z)}{\overline{U}(d)} dz \tag{13}$$

For z $\geq d$, based on boundary layer theory,

$$\frac{q}{d} = \frac{a}{(a+1)(2a+1)} \tag{14}$$

Using the above analogy, the variation of d^* and q along the length of the test section are shown in Fig.5, for a typical test case, where the stabilisation length can clearly be seen.

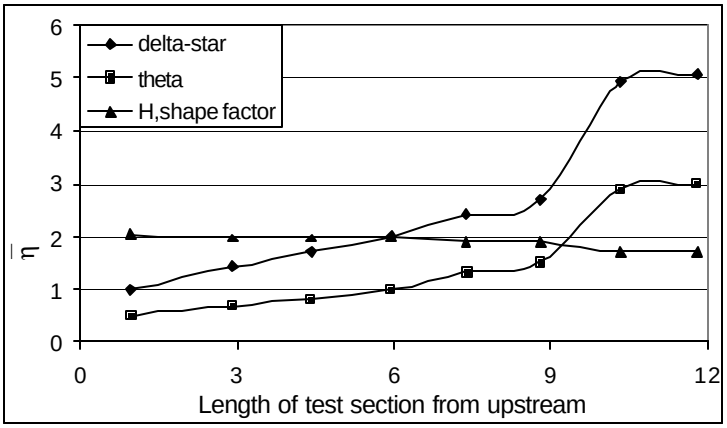

Fig. 5: Variation of Delta-star, Theta and Shape Factor (H) along the Test Section

Evaluation of Shape Factor

Further, the variation of shape factor H, which is defined as the ratio of displacement thickness to momentum thickness (H = d^*/q) is plotted in Fig. 5. The variations shown in the figure are as expected in a boundary layer wind tunnel based on loss of momentum along the working section due to the roughness of the surface. Though the values of d^* and q keep increasing, the fact that H becomes constant at a distance of 10 m from the upstream end implies that the boundary layer is in equilibrium for the remaining length of the test section. Similar trends were observed by other researchers in their respective wind tunnels [Cermak, 1985 and Iyengar 1992]. The experimental data on mean velocity flow characteristics are compared with the results of studies made by other researchers Table 2.

Table 2: Comparison of boundary layer parameters

Parameters	Present study		Cermak [1985]	Cermak [1979]	Rangaraju [1976]	Iyengar [1992]
Terrain	smooth	rough	smooth	Rough	smooth	rough
z_o/δ	5.2x10-4	2.5x10-3	2x10-4	2.2x10-3	5x10-4	2.75x10-3
δ^*/δ	0.124	0.190	0.120	0.170	0.135	0.210
u_* / δ	0.020	0.067	0.023	0.052	0.043	0.063

Turbulence Intensity Profile

The longitudinal turbulence intensity factor, I_u is defined as the ratio of standard deviation velocity u' at any height z to the corresponding mean wind speed at the same height.

$$I_u = \frac{u'(z)}{\overline{U}(z)} \tag{15}$$

A typical profile of I_u along the test section length for 30 cm trip board (test case 2) is shown in Fig. 6.

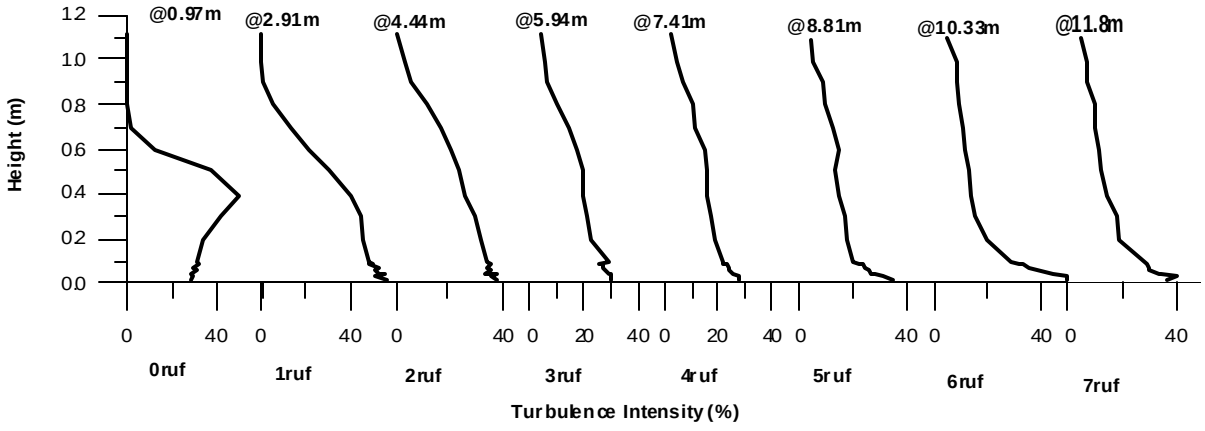

Fig. 6: Variation of Turbulence Intensity along the Test Section

Turbulence Spectra

A typical power spectrum based on FFT analysis is shown in Fig. 7 for 35 cm trip board (test case 3). On comparison with the standard theoretical spectrum, the peak value of the experimental spectrum shifts itself when plotted against reduced frequency, and the spectra collapse onto a curve as shown in Fig. 7. The longitudinal length scale of turbulence is obtained by multiplying the time scale values obtained based on matching the measured spectra with Karman's spectrum. Typically these ranged from 0.5 m to 0.6 m. The above length scale is adequate for model scale ratios of 1:100 to 1:200 for open terrain condition [Simiu & Scanlan, 1986; Robins, 1979]. The formula widely used in wind engineering literature is due to Von Karman has been adopted and is given by [ESDU 1985]:

$$\frac{nS_u(n)}{s_u^2} = \frac{4x_u}{\left(1+70.78x_u^2\right)^{5/6}} \tag{16}$$

where $x_u = (n\, L_u) / U$

L_u = turbulence length scale along the wind direction, u

σ_u^2 = the square of the rms intensity

n = frequency

U = velocity of wind in 'u' direction and

$S_u(n)$ = power spectral density function in frequency domain.

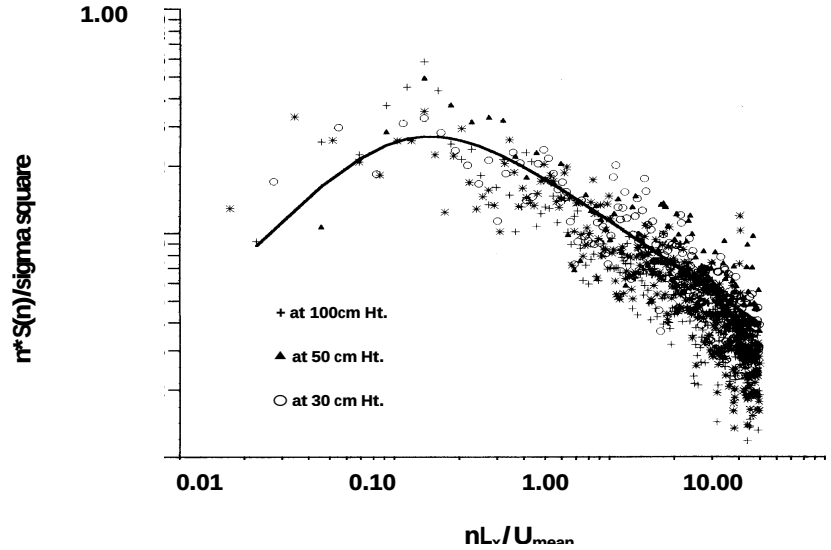

Fig. 7: Typical spectra measured at Test Section

RESULTS AND DISCUSSION

In the present experimental study, an extensive collection of test data had been made on velocity profiles under smooth as well as rough terrain conditions. The top portion of the boundary layer profile was found to be well fitted by the power law, while the lower part of the atmospheric boundary layer was modelled using log-law. Based on the mean velocity profiles using power-law model, the boundary layer thickness, d and the power law exponent a were obtained. For smooth terrain the value of a was found to be about 0.13 to 0.17 and a value more than 0.21 refers to a rougher terrain. Similarly, the value of d varies depending on the scale ratio as well as the vortex generators used for simulation. The values of d as obtained for the test cases

are 0.8m, 1.0m and 1.12m for 20 cm, 30 cm and 35 cm height trip boards, respectively. This shows that sufficient boundary layer depth has been simulated, within which the structural models having geometric scales from 1:50 to 1:250 can be tested in the test section of the tunnel. A typical targeted mean wind speed profile and the corresponding turbulence intensity profile measured at test section for test case (5), representing a simulated scale of 1:250 is shown in Fig. 8.

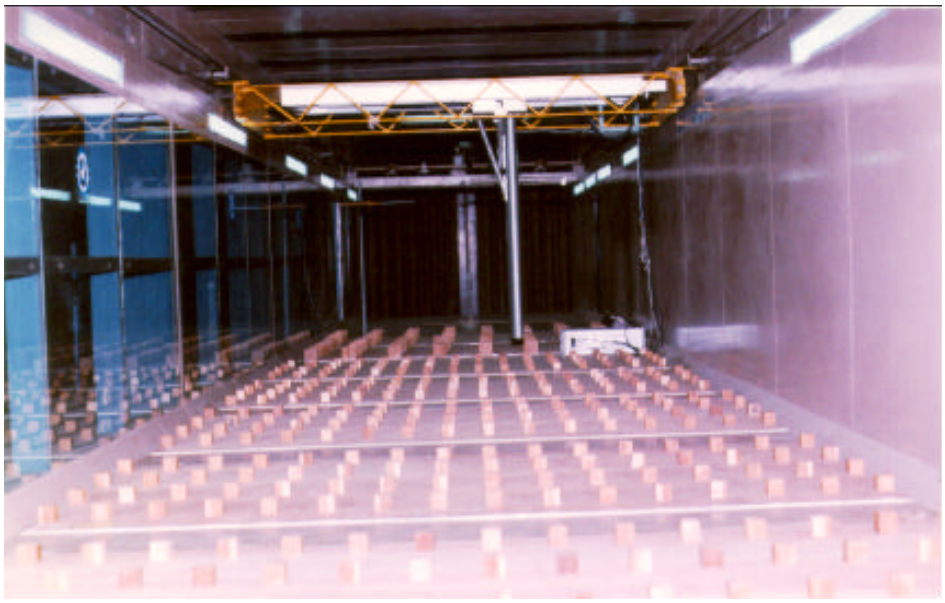

Photo 1: View of Test Section with HWA System

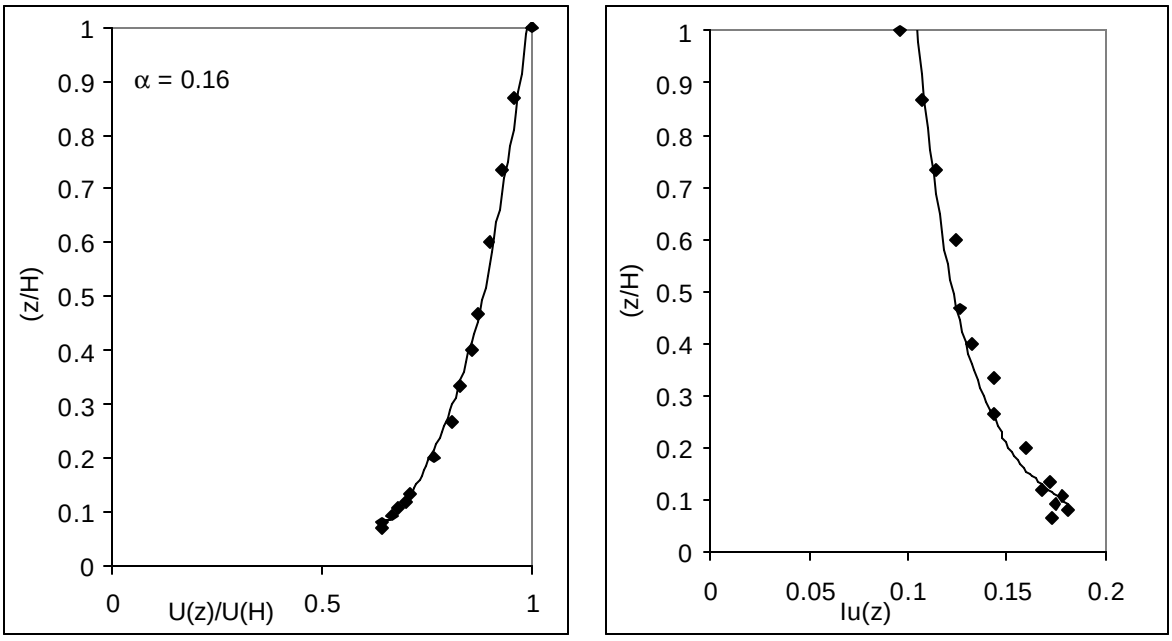

Fig. 8: Target Mean Wind Speed Profile and the corresponding Turbulence Intensity profile measured at Test Section for Test Case (5), representing 1:250 Scale

The aerodynamic roughness length, z_o is one of the parameters used for the determination of scale ratio, based on the full-scale values available in the literature [Simiu & Scanlan, 1986]. For a α value of 0.17, the value of z_o is obtained as 0.0003m in the test. Based on a model scale of 1:100, the full-scale roughness height is obtained as 0.03m. Such a terrain is characterised by open terrain. For α = 0.24, the model roughness height of 0.0026m, corresponds to a full-scale value of 0.26m, which represents an urban terrain. The basis for fixing up the scale ratio is by comparing the wind energy spectrum obtained experimentally with that of a standard spectrum, which has been recommended based on full-scale measurements. The turbulence length scale which is determined as above is a parameter conventionally assumed to check the model geometric scale factor by suitable shift in frequency. Since the turbulence length scale, L_u is a length parameter, it is conveniently expressed in a non-dimensional form, as nL_u/U which is used to describe "reduced frequency". Generally it is assumed that significant energy is available up to 1Hz in full-scale atmospheric boundary layer. The measured spectrum at a given height is matched with Von Karman's spectrum by shifting the reduced frequency axis relative to that of Von Karman spectrum. This shift corresponds to model length scale parameter and it is obtained as the ratio between length scale factors at which the spectra match each other. Accordingly, the model scale factors are deduced.

CONCLUSIONS

The present study is aimed at developing turbulent boundary layer along the test section of a wind tunnel and studying its characteristics using vortex generators. The height of the trip board, T_p is found to be a useful parameter for controlling the values of α and δ . The size of roughening elements is a useful control for turbulence intensity, I_u and for power law exponent, α . Same observations were made by other researchers, when adopting such a system of vortex generators in their respective wind tunnels [Holmes & Carpenter, 1990 and Sundaram et al, 1972]. The present study has enabled in understanding the performance of the boundary layer wind tunnel for simulation of atmospheric boundary layer and is found to be highly satisfactory.

Based on the fully developed turbulent boundary layer characteristics, mathematical model to arrive at different values of α representing different terrains is obtained. Hence, for a selected terrain type (for the values of α ranging from 0.17 to 0.24) and for a chosen scale (for scale factors ranging from 1:50 to 1:250) to be simulated in the wind tunnel, the present investigation provides, the vortex generating system to be adopted to meet the required characteristics of the atmospheric boundary layer.

The trip board provides a certain level of turbulent intensity which does not vary drastically with height, and is the only mechanism by which significant levels of turbulence are realised at upper levels. The roughening elements provided near the floor contribute significantly to intensity of turbulence. However its contribution is only up to 0.5 times height of test section or δ at downstream end. The empirical equations will be very useful for the design of these vortex generators for a given value of power law coefficient. The length scales of turbulence measured on different atmospheric boundary layer profiles indicate that geometric scale ratios of 50 to 250 can be adopted for studies in the wind tunnels. High levels of turbulence of the order of 20 to 25% are possible to generate up to about 25 cm indicating that all low-rise building models can be tested satisfactorily. Also the spectrum shows that "small scale eddies" are preserved which is an important criterion in the determination of peak values of pressures in low-rise building models. The studies conducted enable development of desired boundary layer wind characteristics essential for testing of different types of models in atmospheric boundary layer wind tunnel, which was the main objective of the present investigation.

ACKNOWLEDGEMENT

This paper is being published with the kind permission of director, SERC, Chennai. The technical assistance rendered by the staff of the wind engineering laboratory in conducting the wind tunnel experiment is gratefully acknowledged.

REFERENCES

1. Cermak, J.E. (1979), "Applications of Wind Tunnels to Investigation of Wind - Engineering Problems", AIAA Journal, NY, USA, Vol. 17, No. 7, July, pp. 679-689.
2. Cermak, J.E. (1982), "Wind-Simulation Criteria for Wind -Effect Tests", Proceeding of ASCE Annual Convention, New Orleans, U.S.A., October, pp. 328 - 339.
3. Cermak, J.E. (1985), "Boundary Layer Wind Tunnel for Wind Simulation - Physical Modeling of Wind Effects", Proceedings of Indo-US Workshop on Wind Disaster Mitigation, Madras, India, December, pp. 91-103.
4. Cermak, J.E., and Cochran, L.S. (1992), " Physical Modelling of the Atmospheric Surface Layer", Journal of Wind Engineering and Industrial Aerodynamics, Elsevier, U.S.A., 41-44, pp. 935-946.
5. Cook, N.J. (1985), "The Designer's Guide to Wind Loading of Building Structures: Part 2 - Static Structures", Butterworths, U.K.
6. Counihan, J. (1970), "Further measurements in a Simulated Atmospheric Boundary Layer", Atmo spheric Environment Pergamon Press, Vol.4, U.K., pp. 259-275.
7. Engineering Services Data Unit (ESDU), (1985), "Characteristics of Atmospheric Turbulence near the Ground", Part 2, Data Item: 85020, ESDU International, London.
8. Hansen, S.O., and Sorensen, E.G. (1985), "A New Boundary Layer Wind Tunnel at the Danish Maritime Institute, Journal of Wind Engineering and Industrial Aerodynamics, 18, pp. 213-224.
9. Holmes, J.D., and Osnosphasop, C. (1983), "Flow Behind Two-Dimensional Barriers on A Roughened Ground Plane, and Applications for Atmospheric Boundary Layer Modelling", Eighth Australian Fluid Mechanics Conference, University of New Castle, November, Australia, pp. 11B.13 - 11 B.16.
10. Holmes, J.D., and Carpenter, P. (1990), "The effect of Jenson Number Variations on the Wind Loads on a Low-rise Building", Journal of Wind Engineering & Industrial Aerodynamics, No. 36, pp. 1279-1288.
11. Irwin, H.P.A.H. (1981), "The Design of Spires for Wind Simulation", Journal of Wind Engineering and Industrial Aerodynamics, No. 7, Elsevier, U.S.A., pp. 361-366.
12. Iyengar,Arun K.S. (1992), "Simulation of a Neutral Urban Atmospheric Boundary Layer in the SAFHL BLWT", M.S. Thesis guided by Prof.Cesar Farell, University of Minnesota.
13. Noda, M., Utsunomiya, H., and Nagao, F. (1995), "Basic Study on Blockage Effects in Turbulent Boundary Layer Flows'" Journal of Wind Engineering and Industrial Aerodynamics, 54/55, Elsevier, U.S.A., pp. 645-656.
14. Ranga Raju, K.G., Loeser, J., and Plate, E.J. (1976), "Velocity Profiles and Fence Drag for a Turbulent Boundary Layer along Smooth and Rough Flat Plates", Journal of Fluid Mechanics, Vol. 76, Part 2, pp. 383-399.
15. Reinhold T.A. (1982), "Wind Tunnel Modeling for Civil Engineering Applications", Cambridge, Cambridge University Press.
16. Robins, A.G. (1979), "The Development and Structure of Simulated Neutrally Stable Atmospheric Boundary Layers", Journal of Wind Engineering and Industrial Aerodynamics, Vol. 4, pp. 71-100.
17. Schlichting, H. (1980), "Boundary Layer Theory", Mcgraw Hill Publishing Co. Inc., New York, USA.
18. Simiu, E., and Scanlan, R.H. (1986), "Wind Effects on Structures", John Wiley & Sons, New York.
19. Sivaramakrishnan, S., and Brij Mohan (1992), "Wind and Turbulence Profiles in a Simulated Wind Tunnel Boundary Layer", Mausam, No. 43, India, pp. 283-290.
20. Sundaram, T.R., Ludwig, G.R., and Skinner, G.T. (1972), "Modelling of Turbulence Structure of Atmospheric Surface Layer", AIAA Journal, Vol.10, pp. 743-750.

Journal of Wind and Engineering, Vol. 6, No. 2, July 2009, pp. 30-41

CHARACTERISATION OF AND WIND-INDUCED PRESSURES IN A COMPARTMENTALISED BUILDING DURING A TYPHOON

Kenny C.S. Kwok[a,b] and Peter A. Hitchcock[b]

[a]School of Engineering, The University of Western Sydney, New South Wales, Australia
[b]CLP Power Wind/Wave Tunnel Facility, The Hong Kong University of Science and Technology, Clear Water Bay, Hong Kong

ABSTRACT

A series of experiments was conducted to investigate the behaviour of wind-induced internal pressure in a typical compartmentalised residential apartment in Hong Kong during the passage of a typhoon. Permeability tests were first conducted to quantify the permeability across major leakage paths of the test apartment. Wind-induced external and internal pressures were subsequently measured in test configurations with different internal volumes and different permeability conditions with a dominant windward opening. Mean internal pressures and the resonant frequencies of the fluctuating internal pressures were determined and compared with values predicted from steady-state theory, a Helmholtz resonator and a CFD model. The results showed that the predicted mean internal pressure and the fundamental resonant frequency are in reasonable agreement with the field measurements. Multiple resonant frequencies were also observed in the case of multiple compartments interconnected by internal doorways.

KEYWORDS: Compartmentalised building, permeability, internal pressure, Helmholtz frequency

INTRODUCTION

Extreme winds such as typhoons and thunderstorms exert considerable wind pressures on the external surfaces of buildings. When these wind-induced external pressures act upon an opening in a building, such as when a window in the building is damaged by airborne debris, large internal pressures can be generated which exacerbate the net pressure acting on other parts of the building envelope.

Extensive research on internal pressure inside low rise buildings has been conducted by Holmes (1979, 2001), Liu and Saathoff (1981), Liu and Rhee (1986), Harris (1990), Vickery and Bloxham (1992), Yeatts (1992), Vickery (1994), Sharma and Richards (1997a, 1997b, 2003), Ginger et al. (1997, 2008), Ginger (2000), Oh et al. (2007), Kopp et al. (2008) and others based on theoretical studies, wind tunnel model experiments, field measurements, and comparisons of theoretical models, wind tunnel test results and computational models. Their works have generally demonstrated that internal pressure fluctuations inside a building or building compartment with a specific volume and with a single dominant opening excited by an external pressure pe driven by wind can be modelled by an oscillating air slug across the dominant opening with the following governing equation:

$$\rho_a \mathrm{AI}_e \ddot{x} + \frac{\rho_a \mathrm{A}}{2\mathrm{K}^2} \dot{x} \mid \dot{x} \mid + \frac{g \rho_0 \mathrm{A}^2}{V_0} \mathrm{x} = A \Delta p_e(t) \tag{1}$$

in which, x is the displacement of the air slug; ?$_a$ is the density of the air; le is the length of the air slug; A is the area of the opening; k is the orifice constant and is assumed to have a value of 0.6; ? is the specific heat constant of air; p_o is the pressure already inside the volume (usually taken as the atmospheric pressure), and V_o is volume inside the compartment, respectively.

In terms of internal pressure coefficient C_{pi} and external pressure coefficient C_{pi}, Equation (1) can be rewritten as:

$$\frac{\rho_a I_e V_0}{g \rho_0 A} \ddot{C}_{pi} + \left[\frac{\rho_a V_0 U}{2kgAp_0} \right]^2 \dot{C}_{pi} |C_{pi}| + C_{pi} = C_{pe} \tag{2}$$

in which U is a reference mean wind speed usually taken as the mean wind speed at the top of the building.

The resonant frequency, commonly referred to as the Helmholtz frequency nH of the building volume and dominant opening system is given as:

$$n_H = \frac{1}{2\pi} \sqrt{\frac{gAp_o}{\rho_a I_e V_o}} \tag{3}$$

Dimensional analysis (Holmes 1979, 2001) demonstrates readily that the internal pressure fluctuations for a building volume and dominant opening system can be represented by five dimensionless parameters:

$$\begin{aligned} \pi_1 &= \frac{A^{3/2}}{V_o} \\ \pi_2 &= \frac{p_o}{\frac{1}{2}\rho_a U^2} \\ \pi_3 &= \frac{\rho_a U \sqrt{A}}{\mu} \\ \pi_4 &= \frac{\sigma_u}{U} \\ \pi_5 &= \frac{I_u}{\sqrt{A}} \end{aligned} \tag{4}$$

in which, μ is the dynamic viscosity of air; σ_u standard deviation of longitudinal velocity fluctuations; lu is the integral length scale of turbulence. π_3 is the Reynolds number.

When scaled building models are used to study internal pressures under different model and full-scale test wind speeds, Ginger et al. (2008) have further shown that to maintain correct frequency scaling, the internal volume of the building should be scaled according to $1/[U^2]_r$ in order to cor rectly measure the fluctuating internal pressures.

By combining the governing equation, Equation (2), with the dimensionless parameters given in Equation (4), Ginger et al. (2008) introduced a single dimensionless parameter S* relating opening size to volume:

$$S^* = \left(\frac{a_s}{U_h}\right)^2 \left(\frac{A^{3/2}}{V_{le}}\right) \quad (5)$$

in which a_s is the speed of sound; U_h is a reference mean wind speed taken at the top of the building; and V_{le} is the effective internal building volume taking into consideration leakages. Ginger et al. (2008) further showed, through numerical modelling and re-analysis of field data from the Texas Tech experimental building, that the ratios of standard deviation and peak internal pressures to the external pressures at a dominant windward wall opening are dependent on S*, with the peak internal pressure expected to exceed the peak external pressures by 10% or more for S* greater than about 8.

Hong Kong is frequently visited by typhoons which can cause considerable damage, and even injuries and deaths (e.g. Campbell 2005). The damage to cladding amongst a group of tall office buildings caused by typhoon York in 1999 aroused the attention of the industry towards wind-induced pressures and air-borne debris, and the role of internal pressure on façade loading (Lam et al. 2006). This paper presents the results of a series of field experiments conducted to investigate the behaviour of internal pressure in a typical compartmentalised residential apartment in Hong Kong during the passage of a typhoon.

FEATURES OF THE TEST BUILDING AND TEST APARTMENT

A study was conducted at The Hong Kong University of Science and Technology (HKUST) to examine the wind-induced internal and external pressure in a high-rise building. The Test Building is the Visitor Center situated within the campus of HKUST and it is located on a hillside facing northeast, with a relatively open exposure to winds from the northeast quadrant. The surrounding topography and a cross-section (A-A) of the terrain normal to the Test Building are shown in Figure 1. The Test Building has a height of approximately 30 m above the local ground level and is 140 m above mean sea level. The Test Apartment was the corner apartment situated on the 7th floor of the Test Building, as shown in Figure 2(a). The layout of the Test Apartment reflects the configuration of a typical apartment in Hong Kong featuring rooms separated by brickwork or concrete partitions, as shown in Figure 2(b). Each room is fitted with a solid timber door and ventilation is either provided by windows mounted on an aluminum frame or an independent air conditioning unit. The partitions, doors and windows effectively isolate each room into an individual space with low background permeability and interconnectivity. This type of apartment provides a chance to investigate the effect of permeability on internal pressure over a range of configurations of opened and closed windows and doors.

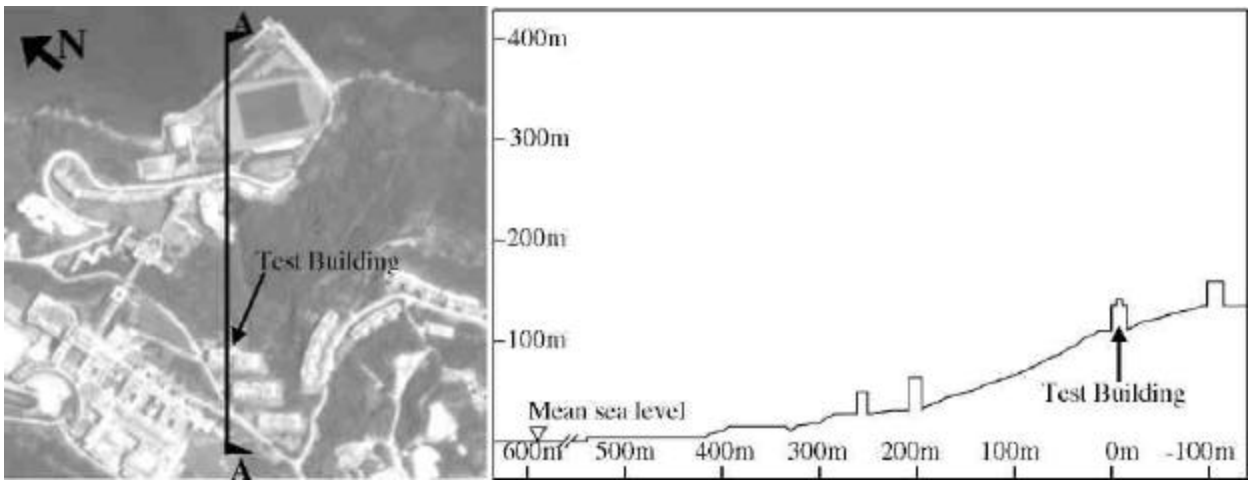

(a) Topographical surroundings (b) Section A-A

Figure 1. Location of Test Building at HKUST.

(a) Test Apartment in the Test Building

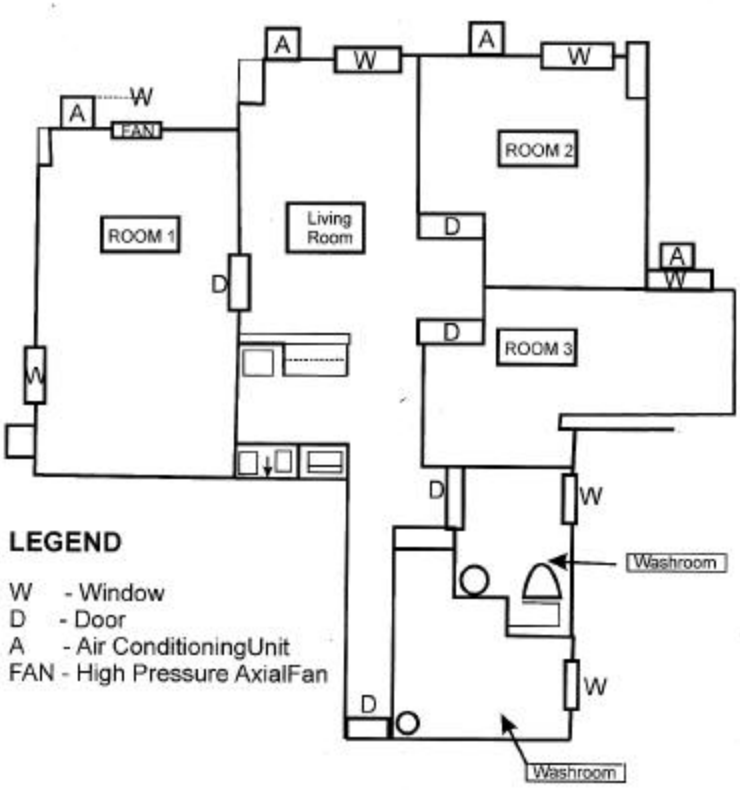

(b) Layout of Test Apartment

Figure 2. Test Building and Test Apartment at HKUST

PERMEABILITY OF THE TEST APARTMENT

The permeability of various leakage paths in the Test Apartment was determined using the test method specified in ASTM E779-03 for determining air leakage rates using controlled fan pressurization and depressurization (Hui et al. 2006a). An axial fan mounted directly onto the north-east facing window frame was used to pressurize or depressurize the test compartment as illustrated in Figure 3(a). The fan power was controlled by a stepless 3-phase frequency inverter to provide a range of flow rates (Q) during both pressurization and depressurization tests. The flow rate was determined with respect to a calibrated reference wind speed representative of the fan-generated velocity profile measured using a thermal anemometer. Pressure differences across the pressurized/depressurized compartment were measured directly by a differential pressure transducer system shown in Figure 3(b) connected by a tubing system which has a flat frequency response up to 30 Hz. Two pressures taps were installed on two flat plates, with one plate-mounted pressure-tap secured to the external wall of the Test Apartment and one inside Room 1, which has an enclosed volume of approximately 36.4 m3. The permeability tests were conducted under virtually a no-wind condition, hence the external wall mounted pressure-tap effectively measured the atmospheric static pressure. The voltage outputs from the pressure transducer were amplified and filtered at 30 Hz and subsequently digitized at a sampling frequency of 200 Hz with 16bit resolution.

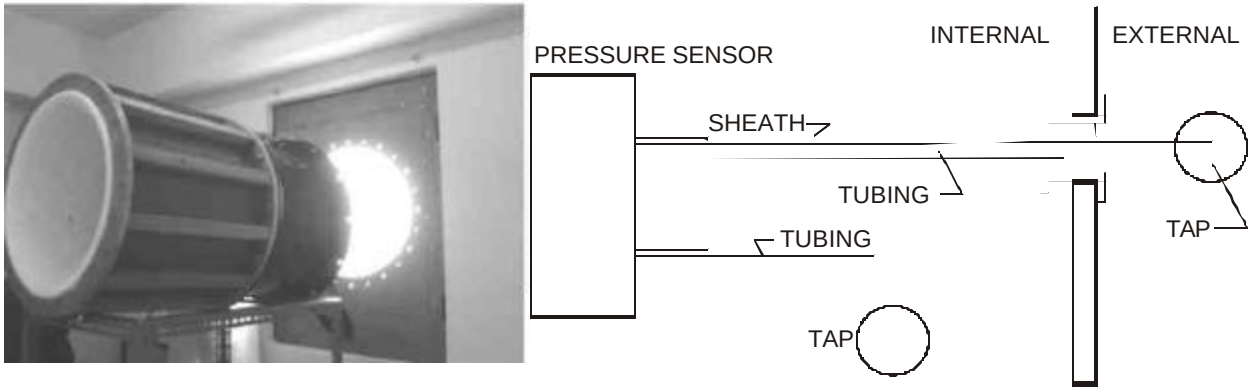

(a) Axial fan and window mounting arrangement (b) Pressure sensor, tap and tubing

Figure 3. Experimental setup for the permeability tests.

Bulk permeability was measured for two test configurations with different internal volumes formed by separate and connecting compartments within the Test Apartment and with different door opening configurations. The two test configurations for the internal volumes of Room 1, i.e. the Master Bedroom, and the whole Test Apartment are illustrated in Figure 4 with the contained internal volumes shaded. These two configurations were first tested with the room door and main door sealed and then un-sealed to isolate the permeability across the leakage paths though the doors. A parametric study (Hui et al. 2006a) has been undertaken to identify the permeability of each leakage path assuming the following flow-pressure relationship:

$$Q = K\sqrt{2(p_e - p_i)/r_a} \tag{6}$$

in which, Q (m^3s^{-1}) is the total flow rate across compartment envelope; p_e (Pa) is the external pressure; p_i (Pa) is the internal pressure; and K is the permeability constant.

(a) Room 1 (b) Whole Test Apartment

Figure 4. Configuration of permeability tests.

The results of the bulk permeability tests and the permeability across each leakage path are plotted in Figure 5(a) and 5(b) respectively. The major leakage paths were found to be the window-mounted air conditioning/ exhaust fan units and the internal and main doors of the Test Apartment. Permeability across these leakage paths during the depressurization tests was found to be slightly higher than that determined during the pressurization tests. However, single permeability constants were able to be estimated across each leakage path and these are summarized in Table 1.

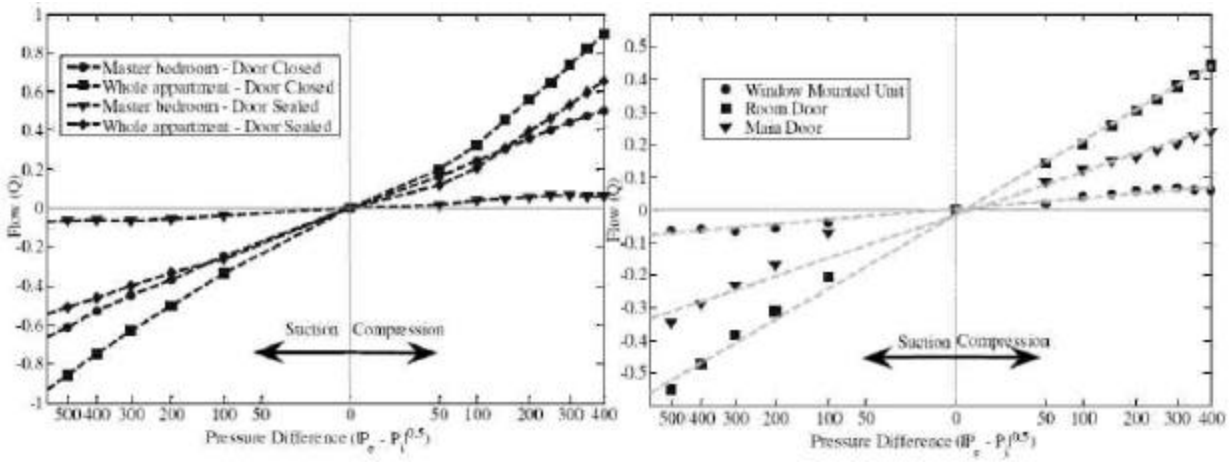

(a) Bulk permeability (b) Permeability across each leakage path

Figure 5. Permeability of Room 1 and Whole Test Apartment.

Table 1. Permeability constants.

	Window-mounted air-conditioning unit	Room 1 Door	Main Door
K (m2)	2.56×10^{-3}	21.56×10^{-3}	10.28×10^{-3}

WIND-INDUCED INTERNAL PRESSURE OF THE TEST APARTMENT

Internal pressure measurements were taken for the two aforementioned test configurations for the Test Apartment during the passage of typhoon Prapiroon that affected Hong Kong for approximately 75 hours in early August 2006. The track of typhoon Prapiroon recorded by the Hong Kong Observatory (Ref. 9, 2006) is shown in Figure 6. During the passage of typhoon Prapiroon, Hong Kong Observatory recorded a maximum gust wind speed of 36.1 m/s (130 km/h) and a maximum hourly mean wind speed of 21.9 m/s (79 km/h) at Waglan Island, an isolated uninhabited island south-east of the main Hong Kong Island where wind data have been measured since 1952. The Test Building at HKUST also experienced a sustained period of strong winds from the exposed north-east quadrant during which pressure measurements were taken both inside and outside the Test Apartment. An ultrasonic anemometer and a specially designed static reference pressure probe were mounted on top of a 5 m tall mast erected near the mid-section leading edge on the roof of the Test Building. Wind tunnel and CFD studies (Hui et al. 2006b, Tsang et al. 2009) have shown that the topography and the proximity of a number of buildings on the upstream slope creates a complex flow regime, with a dominant flow direction that follows closely the slope of the terrain. However, the angle of wind incidence was found to be outside the range that the static reference pressure probe was designed to measure a stable static pressure, hence the reference static pressure was taken from a large vented container housed in a utility closet located in the Test Building on the same floor as the Test Apartment.

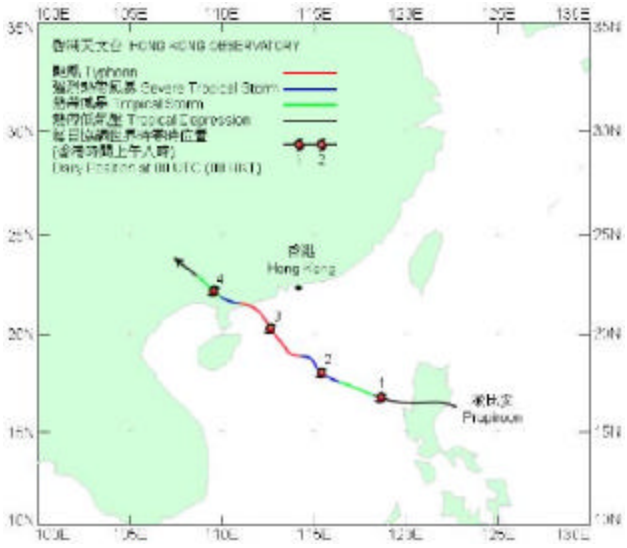

Figure 6. Track of typhoon Papiroon on 31 July to 4 August 2006 [Ref. 9].

External and internal pressures were measured using multiple differential pressure transducers similar to those used in the permeability tests. One plate-mounted pressure-tap was installed immediately beneath the north-east facing window of Room1 which acted as the dominant opening during the experiments. Plate-mounted pressure-taps were installed on the inner walls of Room 1, with one tap installed on the outside of the door to Room 1. Pressures at these pressure-taps were measured against the reference static pressure taken, as mentioned above, from a large vented container housed in the utility closet located on the same floor. These pressures were transferred to the pressure transducers via a tubing system with a flat transfer function and a linear phase response of pressure signals up to 30 Hz. The analog signals output from the pressure transducers were first filtered with a 30 Hz low pass filter and subsequently amplified and digitized at a sampling frequency of 120 Hz for a sample length of 2000 seconds.

Mean Internal Pressure for the Nominally Sealed Compartment

Experiments were undertaken to measure the mean internal pressure inside the nominally sealed test compartment formed by closing the door of Room 1 to isolate the shaded internal volume indicated in Figure 7 and characterised by the measured permeability given in Table 1. The north-east facing window in Room 1 acted as the dominant opening.

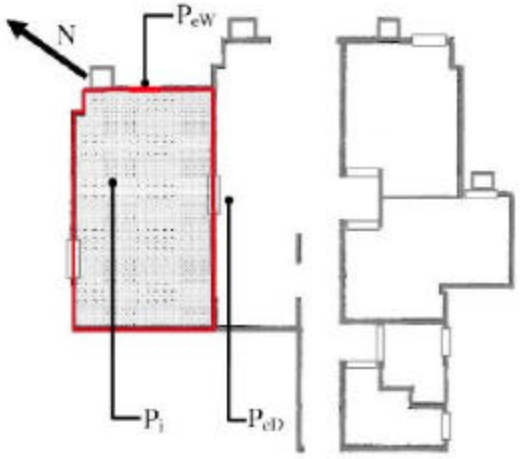

Figure 7. Measurement of mean internal pressure.

Steady-state theory (e.g. Holmes 1979) predicts that, through the conservation of mass, the total flow across a nominally sealed compartment would be zero. Applying Equation (6) to the major leakage paths (i.e. the window mounted air conditioning unit and the bedroom door), the relationship between the steady-state mean internal pressure p_i^s and the external pressures can be predicted by Equation (7):

$$p_i{}^s - p_{ref} = \frac{p_{eW} - p_{ref}}{1+\left(K_D \big/ K_W\right)} + \frac{p_{eD} - p_{ref}}{1+\left(K_W \big/ K_D\right)} \tag{7}$$

in which P_i^s is the measured internal pressure; P_{ref} is the reference pressure; p_{ew} is the external pressure on the window on the windward face; p_{eD} is the external pressure on the Room 1 door; and K_W and K_D are the permeability of the air conditioning unit mounted on the windward bedroom window and the bedroom door respectively.

The measured mean internal pressures, averaged over periods of up to 1000 seconds, can be compared with values predicted by combining Equation (7) and the values measured in the permeability test and summarised in Table 1 ($K_W = 2.56\times10^{-3}$ m^2, $K_D = 21.56\times10^{-3}$ m^2). The results from three measurements (Cases 1 - 3) taken during the passage of typhoon Prapiroon are summarised and compared with the predicted values in Table 2. Generally, the predicted values compare well with the measured values.

Table 2. Measured and predicted mean internal pressure.

	Measured ext. press.		Measured int. press.	Predicted int. press	Discrepancies
	$p_{ew} - p_{ref}$	$p_{eD} - p_{ref}$	$p_i - p_{ref}$	$p_i^s - p_{ref}$	$[(p_i^s - p_{ref}) - (p_i - p_{ref})]/(p_i - p_{ref})$
Case 1	31.2 Pa	25.9 Pa	24.6 Pa	26.0 Pa	5.7 %
Case 2	30.3 Pa	23.7 Pa	24.0 Pa	23.8 Pa	- 0.8 %
Case 3	65.1 Pa	55.3 Pa	51.7 Pa	55.4 Pa	7.2 %

To overcome potential inaccuracies using steady-state assumptions, Harris (1990) modified the governing equations to accommodate the instantaneous flow caused by fluctuating pressure differences between external and internal pressures. However, for the test configurations studied here, the procedure required to determine the instantaneous difference between the internal and external pressure across the window-mounted air conditioning units and the room door is prohibitively complex for practical applications.

Dynamics of Internal Pressure due to a Windward Dominant Opening

Experiments were conducted to investigate the dynamic properties of internal pressure with a windward dominant opening. Two test configurations, the same as were used in the permeability test, were formed by closing the door of Room 1 and the main door of the Test Apartment to isolate two different internal volumes, shaded in Figure 8(a) and 8(b) respectively. For both test configurations, the windward window in Room 1 was opened to form a single dominant opening. The passage of the typhoon was associated with heavy rain bands and hence pressure measurements were only able to be taken during periods when the rainfall eased, thereby limiting the longest sample times to approximately 1000 seconds. Similar to the permeability and mean pressure tests, measurements of differential pressure were taken at a sampling rate of 120 Hz and low pass filtered at 30 Hz. The time histories and spectra of the internal and external pressure signals were analysed to investigate the modifying effects of the test compartment as the external wind pressures were transferred through the single dominant opening to the internal volumes of the two test configurations.

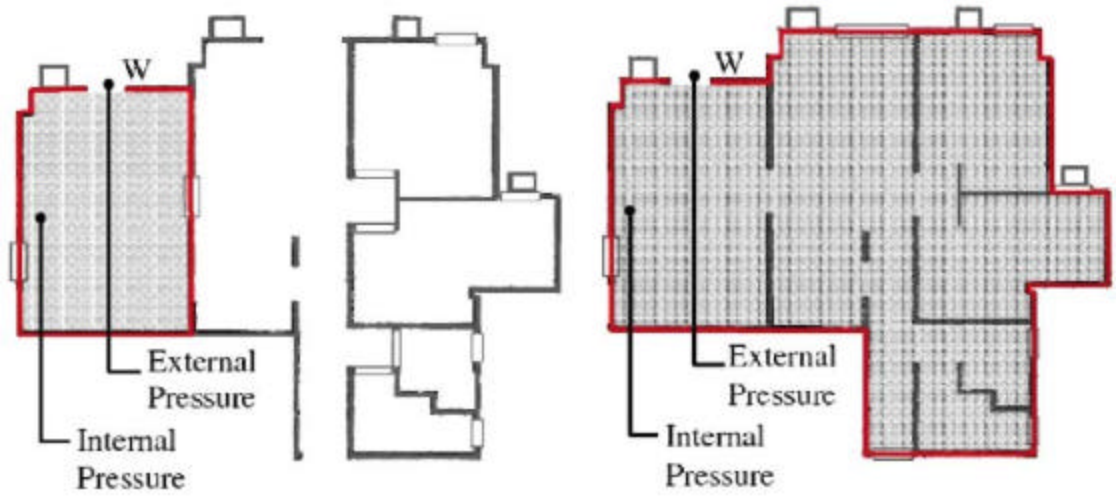

(a) Room 1 (b) Whole Test Apartment

Figure 8. Configurations of internal pressure test with a dominant windward opening marked "W".

A CFD code using finite volume method to solve the Reynolds Averaged Navier-Strokes Equation together with a standard k- model was also employed to study the pressure field in the Test Apartment. The model of Room 1 was first constructed to include the internal as well as external space into the computational domain. The geometry of the model of Room 1 is shown in Figure 9. A constant mass flux inlet with a constant pressure outflow boundary conditions were assumed to provide a compressible flow field simulating the mean flow experienced by the Test Building. The mass flux at the inlet was adjusted to provide the dynamic pressure head observed in full-scale on the windward wall just below the dominant

window opening. To simulate a sudden opening through breaking of the window, the window interface was first defined as a wall to isolate the internal and external volume. The window was then subsequently "removed" by redefining the interface as an internal face. Inlet boundary conditions were applied on the windward window opening through the pressure time history measured during the full-scale experiment.

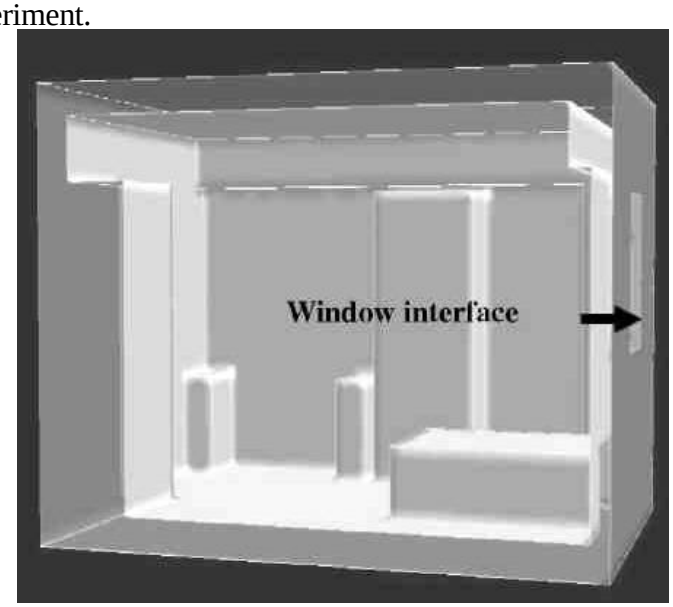

Figure 9. Numerical model of Room 1.

Internal pressure spectra shown in Figure 10(a) highlight a noticeable resonant frequency at 6.8 Hz for the Room 1 only configuration with a windward window opening, followed by a large attenuation at higher frequencies. The resonant frequency agrees reasonably well with the frequency of 8.2 Hz predicted by using Equation (3) and matches closely with that predicted by the numerical model. It is noteworthy that multiple resonant peaks were observed for the Whole Test Apartment configuration with inter-connected compartments, suggesting a more complex system than that for a simple single volume with a single windward opening. The key results for both test configurations are summarized in Table 3.

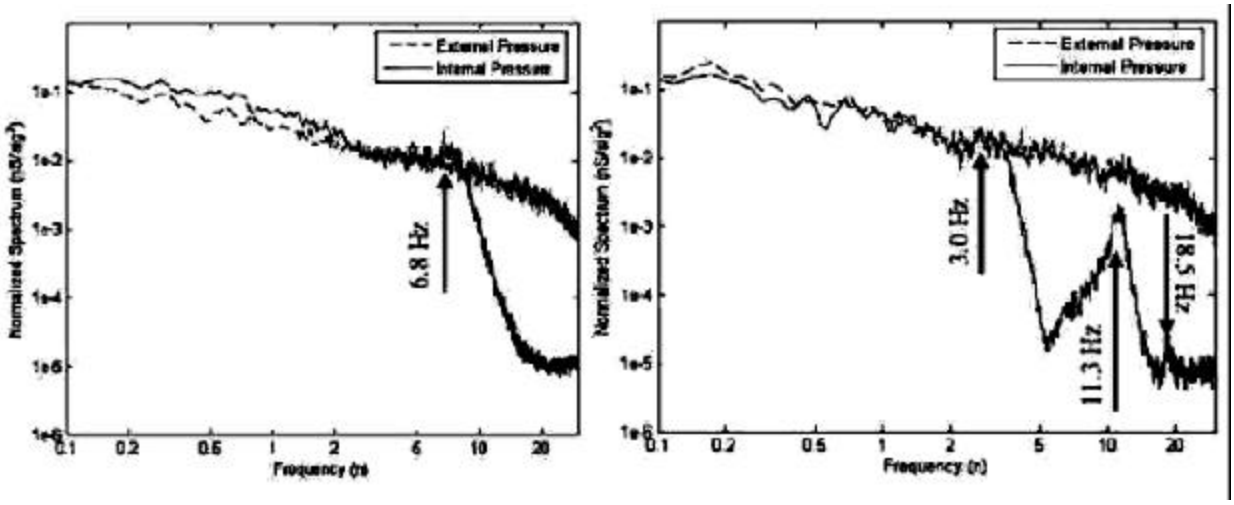

(a) Room 1 only (b) Whole Test Apartment

Figure 10. Normalized spectra of internal and external pressures.

Table 3. Summary of measured and predicted resonant frequency.

	Room 1	Whole Test Apartment
Opening area	0.682m^2	0.682m^2
Enclosed volume	36.4m^3	139.9m^3
Resonant frequency		
i) Measured	6.8Hz	3.0Hz/11.3Hz/18.5Hz
ii) By Equation (3)	8.2Hz	3.2Hz
iii) By CFD model	6.3Hz	-

It is noteworthy that the measured resonant frequencies for Room 1 only and for the whole Test Apartment are all well above 1 Hz, which are outside the energy containing frequencies of the wind spectrum and the corresponding wind-induced external pressure spectrum. Hence these typical compartmentalised apartments are not expected to produce significant internal pressure amplifications due to wind-induced external pressure fluctuations at typical window openings found in these apartments.

CONCLUSIONS

The behaviour of internal pressure in a typical compartmentalised residential apartment was studied during the passage of a typhoon. A permeability test was first carried out to determine the permeability constants through major leakage paths in two test configurations: a single room and multiple interconnected rooms. Wind-induced internal pressures and external pressures of the test apartment were measured during the passage of a typhoon. For the nominally sealed single room configuration, the mean internal pressures predicted by steady-state theory were found to be in reasonably good agreement with measured internal pressures.

The dynamics of the wind-induced internal pressures were also studied in the frequency domain with a windward dominant opening for both test configurations and resonant frequencies were observed in both cases. While a Helmholtz resonator model predicted the resonant frequency for the single room configuration reasonably accurately, multiple resonance peaks were observed in the internal pressure spectrum for the multiple room configuration, highlighting the more complex mechanisms associated with a multiple compartment configuration with multiple leakage paths.

The measured resonant frequencies for the single room only and for the multiple interconnected rooms are all well above 1 Hz, which are outside the energy containing frequencies of the wind spectrum and the corresponding wind-induced external pressure spectrum. Hence these typical compartmentalised apartments are not expected to produce significant internal pressure amplifications due to wind-induced external pressure fluctuations at typical window openings found in these apartments.

ACKNOWLEDGEMENTS

This research is supported by the Research Grants Council of Hong Kong (Project: HKUST 6293/03E). The contribution of Mr Desmond Hui is gratefully acknowledged. Thanks also go to the staff of the CLP Power Wind/Wave Tunnel Facility at HKUST for their assistance with this research.

REFERENCES

1. ASTM E799-03(2003), Standard Test Method for Determining Air Leakage Rate by Fan Pressurization, ASTM International.
2. Campbell, S. (2005), "The History of wind damage in Hong Kong", Wind Engineering Research Centre, Graduate School of Engineering, Tokyo Polytechnic University, Japan.

3. Ginger, J.D. (2000), "Internal pressure and cladding nett wind loads on full scale low-rise building", Journal of Structural Engineering, ASCE, Vol. 126, pp. 538-543.
4. Ginger, J.D., Mehta, K.C. and Yeatts, B.B. (1997), "Internal pressures in a low-rise full scale building", Journal of Wind Engineering and Industrial Aerodynamics, Vol. 72, pp. 163-174.
5. Ginger, J.D., Holmes, J.D. and Kopp, G.A. (2008), "Effect of building volume and opening size on fluctuating internal pressures", Journal of Wind and Structures, Vol. 11, No. 5, pp. 361-376.
6. Harris, R.I. (1990), "The propagation of internal pressures in buildings", Journal of Wind Engineering and Industrial Aerodynamics, Vol. 34, pp. 169-184.
7. Holmes, J.D. (1979), "Mean and fluctuating internal pressures induced by wind, Proceedings of 5th International Conference of Wind Engineering, Fort Collins, Pergamon Press, Oxford, Vol. 1, pp. 435-450.
8. Holmes, J.D. (2001), Wind Loading of Structures, Spon Press, pp. 128-138.
9. http://www.weather.gov.hk/publica/tc/tc2006/english/figure331.htm
10. Hui, D.K.K., Campbell, S., Hitchcock, P.A. and Kwok, K.C.S. (2006a), "Permeability measurement on a typical Hong Kong apartment", Proceedings of 12th Australasian Wind Engineering Society Workshop, Queenstown, New Zealand.
11. Hui, D.K.K., Hitchcock, P.A. and Kwok, K.C.S. (2006b), "Developing a static pressure reference probe", Proceedings of 12th Australasian Wind Engineering Society Workshop, Queenstown, New Zealand.
12. Kopp, G.A., Oh, J.H. and Inculet, D.R. (2008), "Wind induced internal pressures in houses", Journal of Structural Engineering, ASCE, Vol. 134, pp. 1129-1138.
13. Lam, K.M., To, Alex P. and Guo, D.J. (2006), "Wind Tunnel Study of Peak Wind Pressure on Government Towers in Wanchai during Typhoon York 1999", HKIE Transactions, Vol. 13. No. 3, pp. 17-22.
14. Liu, H. and Saathoff, P.J. (1981), "Building internal pressure: Sudden change", Journal of the Engineering Mechanics Division, ASCE, Vol. 107, No. EM2, April, pp. 309-321.
15. Liu, H. and Rhee, K.H. (1986), "Helmholtz oscillation in building models", Journal of Wind Engineering and Industrial Aerodynamics, Vol. 24, pp. 95-115.
16. Oh, J.H., Kopp, G.A. and Inculet, D.R. (2007), "The UWO contribution to the NIST aerodynamic database for wind loads on low buildings: Part 3, Internal pressures", Journal of Wind Engineering and Industrial Aerodynamics, Vol. 95, pp. 755-779.
17. Sharma, R.N. and Richards, P.J. (1997a), Computational modelling in the prediction of building internal pressure gain functions, Journal of Wind Engineering and Industrial Aero dynamics, Vol. 67-68, pp. 851-852.
18. Sharma, R.N. and Richards, P.J. (1997b), "Computational modelling of the transient response of building internal pressure to a sudden opening, Journal of Wind Engineering and Industrial Aerodynamics, Vol. 72, pp. 149-161.
19. Sharma, R.N. and Richards, P.J. (2003), "The influence of Helmholtz resonance on internal pressures in a low-rise building, Journal of Wind Engineering and Industrial Aerodynamics, Vol. 91, pp. 807-828.
20. Tsang, C.F., Kwok, K.C.S., Hitchcock, P.A. and Hui, D.K.K. (2009), "Large-eddy simulation and wind tunnel study of flow over an up-hill slope in a complex terrain", Journal of Wind and Structures, Vol. 12, No. 3, pp. 219-238.
21. Vickery, B.J. (1994), "Internal pressures and interactions with the building envelope", Journal of Wind Engineering and Industrial Aerodynamics, Vol. 53, pp. 125-144.
22. Vickery, B.J. and Bloxham, C. (1992), "Internal pressure dynamics with a dominant opening", Journal of Wind Engineering and Industrial Aerodynamics, Vol. 41, pp.193204.
23. Yeatts, B.B. (1992), Internal pressure for buildings, MSc. Thesis, Texas Tech University.

Journal of Wind and Engineering, Vol. 6, No. 2, July 2009, pp. 42-50

NUMERICAL SIMULATION OF TURBULENT FLOW PAST A CONICAL WATER TANK STRUCTURE

M. Jayakumar[1], Rajani[2], Sekhar Majumdar[2], K.M. Parammasivam[3]

[1]Dept. of Aerospace Engineering, MIT, Chromepet, Chennai - 600 044.
email: Jayakumar.M2@in.bosch.com
[2]Computational and Theoretical Fluid Dynamics Division, NAL, Bangalore - 560 037
[3]JSPS Fellow, Tokyo Polytechnic University, Japan.

ABSTRACT

Water tanks are usually reinforced concrete structure of circular or rectangular cross section, supported on another very tall cylindrical tower type structure. Extensive measurement and numerical computations on flow past prismatic cylinders, reported in unclassified literature, have clearly established that beyond a critical flow Reynolds number, time-dependent fluctuating forces are induced on the cylinder due to alternate vortex shedding. In most of the practical situations, these towers, standing on a rough uneven terrain, are partially or totally immersed in the relatively thick oncoming atmospheric boundary layer. The present work aims at simulating numerically the three-dimensional turbulent flow around a water tank in the shape of a frustum of a cone, mounted on a cylindrical structure of circular cross section for a typical flow Reynolds number of 1.05 million. Some of the characteristic structure of the flow past the tower has been identified from the numerical visualisation of the instantaneous and time-averaged flow field.

Key Words: Water Tank Tower, Numerical Simulation, Visualisation

INTRODUCTION

Water tanks are tall slender structures with large masses on top and this type of structure is constructed in all terrains mainly to ensure adequate supply of water to colonies and industrial buildings. Wind load acting on these types of tank-towers are determined by the characteristics of the oncoming flow, the tower geometry and the features of the surrounding terrain. The mean flow conditions upwind of tall slender structures are usually not uniform since the mean flow velocity increases with height in the atmospheric boundary layer. In most of the practical situations, the towers are partially or totally immersed in the relatively thick boundary layer of the oncoming flow past the towers standing on a rough uneven terrain. Especially freestanding water tank towers constructed in the coastal regions are exposed to extreme winds due to cyclones and so special attention must be paid in their design and construction. The vast majority of investigations has been carried out for the flow around a cylinder of circular cross section, although the structures of engineering interest like water tank towers, chimneys etc., are not necessarily of circular cross section. Wind tunnel measurement data available on scaled down models of cylinders of varying cross-section are also extremely limited and that too mostly for the time-averaged pressure and aerodynamic forces on the cylinder surface. More in-depth investigation is therefore needed to have a better understanding of the physics of unsteady flow around non-streamlined bodies of arbitrary cross section.

LITERATURE REVIEW AND APPROACH

The computation uses an implicit pressure-based finite volume type Navier Stokes solver in generalized non-orthogonal curvilinear coordinates, developed (Majumdar and Rajani, 1999) in the CTFD Division, NAL Bangalore. The grid with appropriate geometric stretching in the near wall zone is generated by a Differential - Algebraic Hybrid method (Zhu, Rodi and Schönung, 1989) which involves the numerical solution of the elliptic type differential equations at a coarse level, followed by an algebraic (bicubic spline) interpolation procedure to obtain the fine grid from the coarse level. The flow solution algorithm based on the pressure-velocity solution strategy similar to the well-known SIMPLE algorithm of Patankar & Spalding (1972), employs non-orthogonal, boundary-fitted multiblock structured grids and collocated variable arrangement. Eddy viscosity based k- turbulence model with near wall damping function approach of Chien (1982) is used for simulation of turbulence.

In order to assess the accuracy of the numerics as well as the adequacy of the turbulence models used in the RANS solver, computations have been first carried out for laminar as well as turbulent flow past a circular cylinder for typical Reynolds numbers of 3900 for which extensive measurement data and other numerical simulation results are available for validation. Finally turbulent flow over a conical water tank tower at Reynolds number based on the tank top diameter as 1.05×10^5 has been analysed for both uniform and non-uniform oncoming flow and compared with the measurement data of Parammasivam[7] (2005) et al.

NUMERICAL SOLUTION OF FLOW EQUATIONS

The present algorithm uses non-orthogonal coordinates with Cartesian velocities and the equations for instantaneous fluid motion for incompressible flow may be written in a generalised form as follows:

$$\frac{\partial (r f)}{\partial t}+\frac{\partial}{\partial x_i}\left(C_{if} + D_{if} \right) = JS_f \tag{1}$$

where, J is the Jacobian transformation and for any dependent variable f, the terms Ci_f, Di_f and S_f relate to convection, diffusion and source terms and i is the summation index over three directions *(i = 1, 2, 3)*.

Computation Scheme

The present method solves the set of the discretised equations for the complete domain using an iterative algorithm sequentially, taking one equation at a time. The iteration takes care of both the strong coupling amongst the equations as well as the non-linearities involved. The linearised form of equation to be solved for a variable f with implicit under relaxation is:

$$f_p = \frac{\sum A_{nb} f_{nb} + SU + (1-a_f) f_p^0 A_p}{A_p / a_f} \tag{2}$$

The unknown f in these equations are the three Cartesian velocity components, the pressure correction that modifies the pressure and velocity field after every iteration, the kinetic energy of turbulence and its dissipation rate for turbulent flows. Since the equations are non-linear, the coefficients A_{nb} are functions of the dependent variables themselves and the algorithm must provide effective means for calculating these

coefficients. Strictly speaking, such coupled non-linear system of equations need simultaneous solution of all the variables. But the iterative algorithm used in the present code updates the variables in a sequential (decoupled) manner and the solution is arrived at iteratively.

RESULTS AND DISCUSSION

Flow past a Circular Cylinder

The size of the computational domain for 2D simulation is 63x144 grids for each block as shown in Figure 1(a). The grids are stretched radially near the wall (? r = 0.0001D) to resolve the local sharp gradients of the flow variables. For 3D simulation, the computational domain considered is similar as in 2D computation except that there are 32 nodes along the span wise direction covering a distance of $2p$. The numerical grid and the initial conditions used for this calculation at Re = 3900 is shown in Figure 1(a) and Figure 1(b). The computation is carried out for both laminar flow and turbulent flow using Chien turbulence model. Table 1 shows the comparison of Strouhal number $\left(St = \frac{fD}{V} \right)$, Cl_{RMS}, Cd_{AVG} and Cd_{RMS} with the available measurement data, where lift-coefficients is expressed as, $C_l = \frac{1}{2}\int_0^{2p} C_p(q)\sin(q)\partial J$ and drag-coefficient is expressed as $C_d = \frac{1}{2}\int_0^{2p} C_p(q)\cos(q)\partial J$ and C_p is the pressure coefficient $\left((p - p_\infty) \Big/ \frac{1}{2} r U_\infty^2 \right)$. In the above equations, integral 0 to $2p$ represents the length of the cylinder. So the lift and drag coefficient is calculated for the entire length of the cylinder for 3D simulation.

Table 1 Comparison of Strouhal number, Cl_{RMS}, Cd_{AVG} and Cd_{RMS}

Study ±	Re = 3900			
	2D-Laminar	2D-Turbulent	3D-Turbulent	Measurement (Norberg, 1987)
Strouhal number	0.234	0.195	0.195	0.2 - 0.22
Cl_{RMS}	1.2	0.54	0.521	-
Cd_{AVG}	1.58	1.15	1.079	0.98 0.05
Cd_{RMS}	0.26	0.046	0.036	-

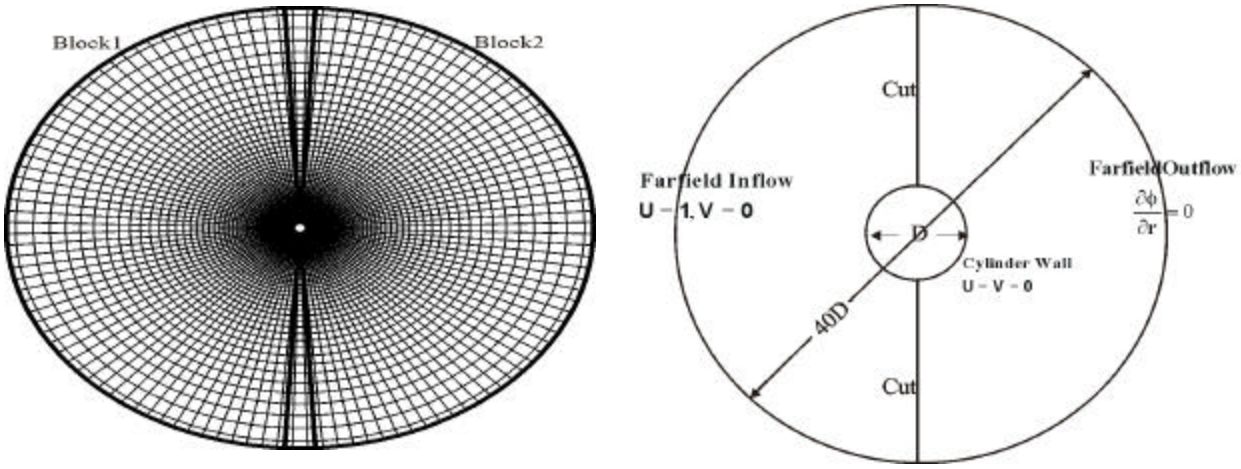

(a) 2-block grid (63x144) arrangement with overlapping control volumes

(b) Boundary condition

Fig. 1 Computation of Flow Past Circular Cylinder

The computed time averaged pressure coefficients are compared to available measurement data at Re=3900 in Figure 2. The surface pressure at the forward stagnation point is well captured and it agrees well with the experiment. Beyond the suction peak, the flow gets separated and the pressure starts increasing. The prediction of backpressure in laminar computation is not good, because the turbulent flow is computed as laminar flow. When the flow is computed with a turbulence model, there is no significant difference between the 2D and 3D turbulent simulations. In relation to the experimental data of Norberg (1987) the turbulent simulation results even with discrepancies are found to be slightly better than the laminar results.

Figure 3 shows the mean stream wise velocity along the centerline for turbulent simulations. Experimental data due to Krothapalli et al (1994) are included. The data agree fairly well in the near cylinder region, but there are large differences in the wake region.

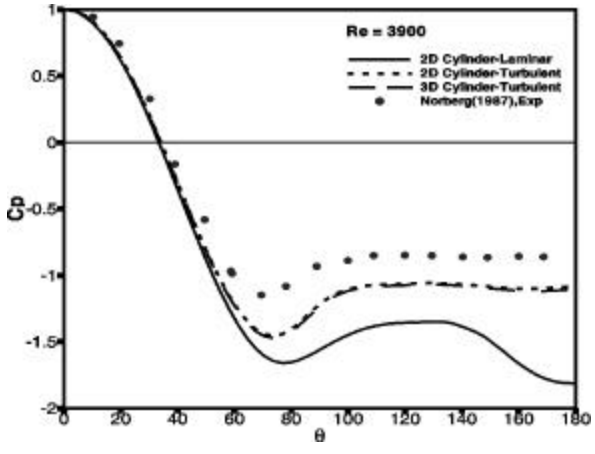

Fig. 2 Time averaged surface pressure around the cylinder

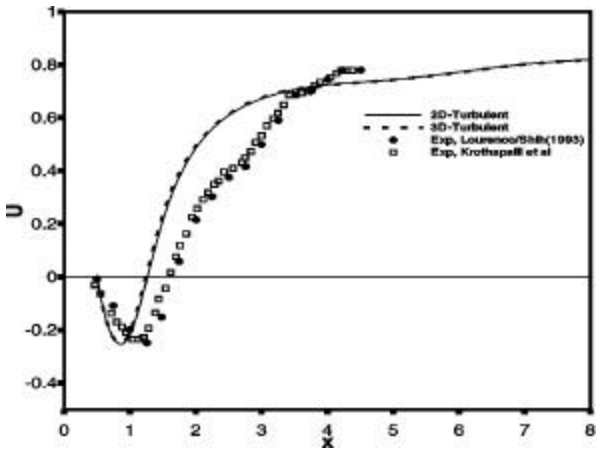

Fig. 3 Mean Streamwise velocity along the wake centerline

Turbulent Flow around Water Tank Tower

The computation uses simple 2D boundary-fitted curvilinear grid with 135 nodes covering the vertical cross section of half of the tank and 65 nodes along the radial direction. Such 2D cross sectional planes are circumferentially stacked on 60 numbers of meridional planes, spaced at interval of 6^0 along the periphery of the tower as shown in Figure 4. The boundary layer developing on the curved tower wall surface has been resolved by at least 8 to 10 points along the wall normal direction, before the separation takes place. Using the above-mentioned grid, the value of the dimensionless near wall distance $y^+ = \frac{y}{\nu}\sqrt{\frac{t_w}{r}}$ is maintained below about 15 for the first near wall node on the tower top surface or near the tunnel floor surface whereas $y+$ did not exceed 35 anywhere near the curved tower surface. Calculations have been carried out with two different inlet velocity profiles - (i) uniform profile of the free stream velocity along the tower height and (ii) simulated atmospheric boundary layer profile obtained from tunnel measurement data. The power law exponent of $\alpha = 0.27$, obtained from tunnel measurements (Parammasivam, 2005) has been used for specifying the mean velocity profile of the oncoming boundary layer. The boundary condition is shown in Figure 5.

Characteristic features of the Flow Field

Figure 6 shows the computed particle traces based on the flow velocity components u (along x) and w (along z) on the vertical midplane (x-z) parallel to the flow (y = 0), formed by one plane from each block on either side of the tank tower axis. It is clear from the figure that the approaching flow turns downward all along the conical as well as the cylindrical shaft section of the tower. This perhaps may be attributed to the finite height of the tower and also to the formation of a low-pressure vortical zone near the upstream side at the foot of the tower where the oncoming boundary layer decelerates and separates in the strong adverse pressure gradient created by the stagnation effect. The small vortical structure generated on the tower top due to flow separation at the sharp edge of the cone base, observed clearly in Figure 6(a), causes a local low static pressure at this vortex center which eventually drives the flow upwards along the cone surface only for a very small length, close to the cone top edge. The small separation bubble reattaches nearly at a length of about 0.1D from the separating edge, where D is the diameter at top of the conical water tank tower.

The variation of the mean separation point location on the tower surface along the height of the tower is shown in Figure 7. The separation location is observed to be approximately at around 155 from the front stagnation point over the central portion ($0.2 < z/H < 0.5$, where H=1.438D) of the cylindrical shaft of the tower. Both near the ground and near the location of cylinder-cone transition, the separation point is shifted upstream whereas the shift is more in magnitude near the ground. Near the top surface of the tower the separation point again drifts further downstream, very close to the rear stagnation point. This upstream shift of the separation location near the ground and also near the cone-cylinder junction is most likely associated with the vertically downward fluid motion due to the formation of the longitudinal

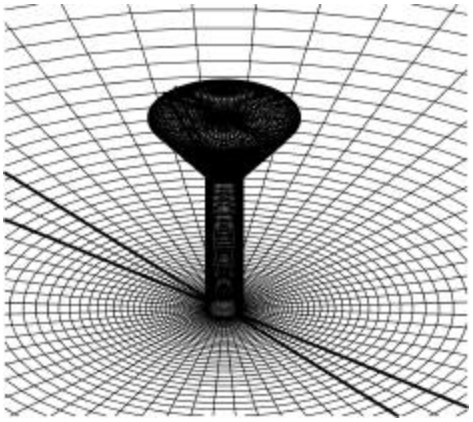

Fig. 4 Grid on tank surface and on the terrain surface

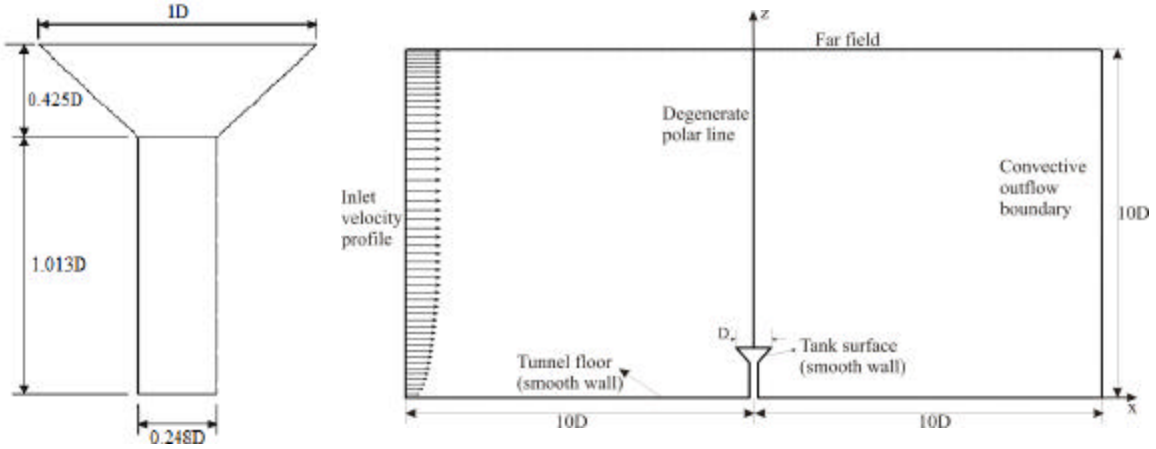

Fig. 5 Tank Dimensions and Boundary conditions for flow past a tank tower structure

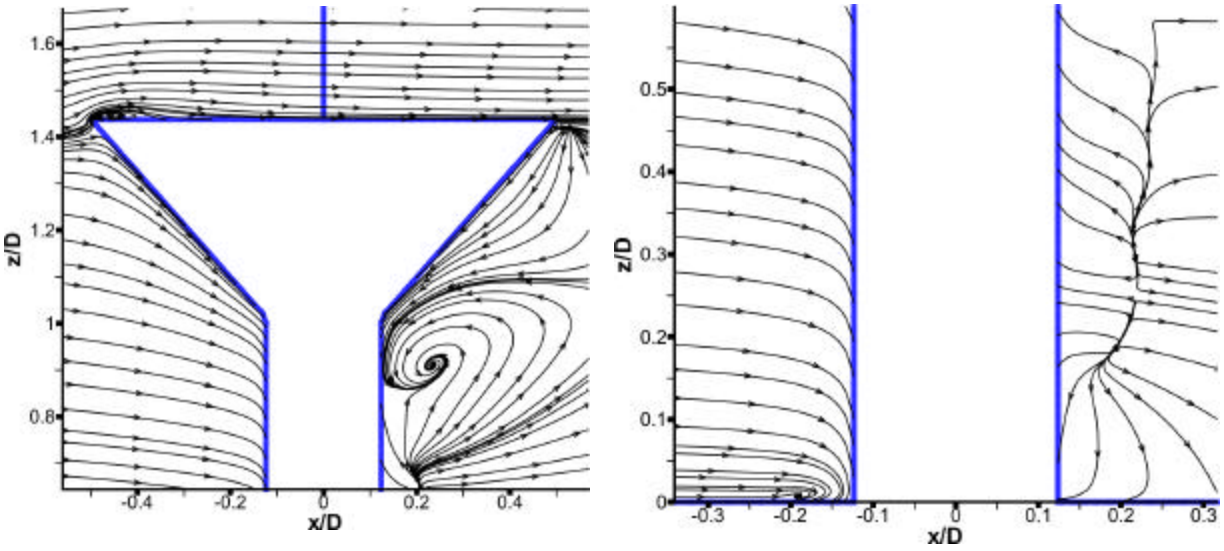

(a) Top of the tank tower **(b) Bottom of the tank tower**

Fig. 6 Particle trace on a vertical mid plane (y = 0)

horse-shoe vortex near the foot of the tower and the presence of another stream wise vortical structure in the vicinity of the junction respectively. On the other hand, near the tower top sections, the downstream shift of the separation point on the curved surface of the tower may be attributed to the formation of the streamwise vortex spinning off the roof edge, shown later in Figure 8. Similar upstream shift of separation point at sections near the end planes of the cylinder relative to those at the middle part for flow past a surface mounted circular cylinder of finite height has been earlier reported by computation of Majumdar et al (1989).

Cross Planes normal to the flow in the Tower Wake

Figure 8 shows the computed particle traces based on cross flow velocity vectors (*v* and *w* only) on a cross plane in the downstream wake (*x/D* = 1.0) of the tower. The magnitudes of the secondary velocities (*v* and *w*) on these planes are obviously small compared to the longitudinal velocity (*u*); but the particle traces clearly indicate some of the important cross flow structures in these figures. Two contra-rotating streamwise vortex pairs are clearly observed on this cross plane - one originated near the edge dividing the cylindrical and conical section of the tower and another is the so-called horse-shoe vortex near the foot of the tower. The cross flow particle traces near the cone curved surface are also observed to be nearly normal to the cone surface and fluid is entrained from the surrounding by the jet kind of flow along *x*-direction over the tank top surface. All the three streamwise vortices are gradually stretched and weakened in strength along the downstream direction due to the viscous and turbulence dissipation effect and finally disappear.

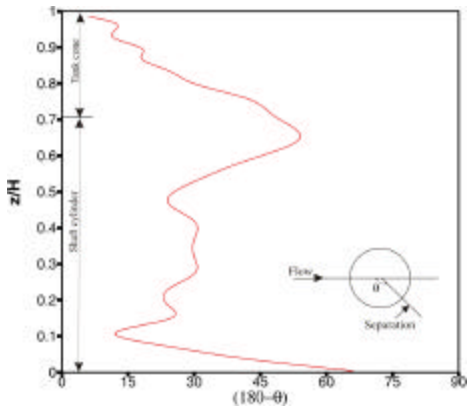

Fig. 7 Variation of separation point location along the height of a tank tower

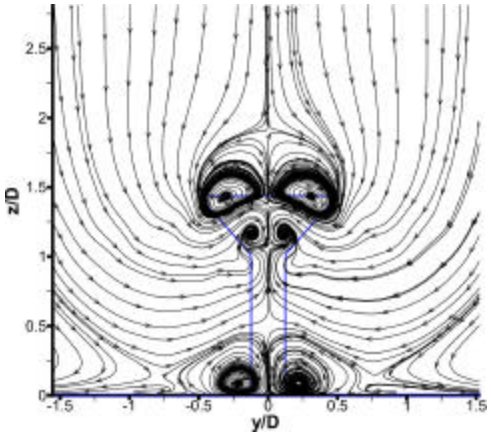

Fig. 8 Particle traces on cross planes in the wake

Surface Pressure Distribution

Figure 9 compares the computed and the measured time-averaged pressure distribution around the tower periphery. The predicted distribution is shown for both uniform free stream velocity and the simulated boundary layer profile at the inlet plane and the results using boundary layer profile are found to be in better agreement with measurement data than those of the uniform inlet velocity flow. In general at all levels of the tower, the pressure reaches a maximum value near the front stagnation point and then drops as the flow is accelerated around the front part till a suction peak is reached at around $\theta = 90^0$. Beyond this point, the pressure rises again leading to separation of the boundary layer in the adverse pressure gradient zone at a location decided by the local flow condition, which obviously is not the same at different levels of the tower. The measurement data shows that after separation, a pressure plateau is formed when the static pressure levels off almost up to the rear stagnation point ($\theta = 180^0$), to an almost uniform level known as the *Base Pressure* in the terminology for flow past circular cylinder. At low values of *z/D* = 0.144 the stagnation

pressure and the suction peak of the pressure variation are reasonably well predicted when the simulated boundary layer profile is used as inflow to the computation domain. In the conical section also, the predicted stagnation pressure is observed to be maximum at $\theta = 0^0$ only and the magnitude is much larger than the corresponding measured pressure at the same location. Very large discrepancies are observed between the prediction and measurement especially in the base pressure level which eventually decides the drag coefficients at different sections of the tower. Large discrepancies are observed between measurement and prediction even in the magnitude and location of the minimum pressure on the tower surface. Such discrepancies clearly indicate that the boundary layer prior to separation, which happens to be laminar at the present range of flow Reynolds number, has not been adequately resolved by the present grid normal to the surface. The Fast Fourier Transform (FFT) for the whole Tank structure gives the lift coefficient (C_l) along *y*-direction a mean value of zero, as expected physically with an rms fluctuation of 0.0012. The Strouhal number $\left(St = \frac{fD}{V} \right)$ based on the maximum diameter of the cone top is 0.156 whereas the measured Strouhal number on the tunnel model reported by Parammasivam (2005) is 0.133. The FFT for the whole Tank structure gives the drag coefficient (C_d) along *x*-direction a mean value of 0.114 with an rms fluctuation of 0.0074.

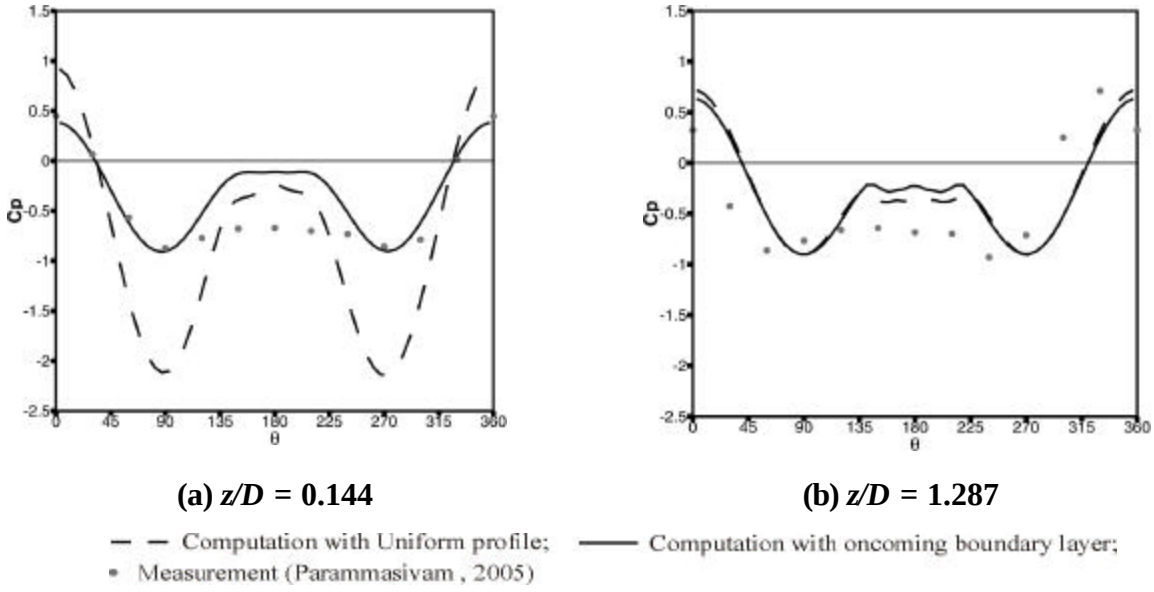

Fig. 9 Surface pressure at different horizontal cross sections

CONCLUSION

Computation of the flow past the water tank tower model is carried out with the *k-e* turbulence model, coupled to standard logarithmic law of wall only due to limitation of the present computational resources. The computation results have established that many of the complex flow features in the vicinity of such tall tower structures of circular cross section, immersed in a boundary layer may be simulated in a realistic manner. Some of the predicted flow features include the formation of horse-shoe vortex, flow separation and vortex shedding from the curved tower surface, flow separation at the leading edge of the tower top surface, the formation of the three distinct longitudinal vortex systems generated on cross planes normal to the free stream flow direction. The surface pressure distributions at different tower heights have however shown that the grid resolutions along radial as well as circumferential direction are inadequate and too crude to capture the correct laminar flow separation on the curved surface. The use of the logarithmic law of wall has also

been quite inadequate to capture the correct location of separation and hence to predict the post separation behavior of the flow including vortex shedding.

REFERENCES

1. Chien, K. Y. (1982),"Predictions of channel and boundary layer flows with a low Reynolds number turbulence model", AIAA Journal, Vol. 20, No. 1., pp.33-38.
2. Krothapalli, A, Shih, C. and Lourenco, L. (1994),"The Near Wake of a Circular Cylinder at 0.3<M?<0.6: a PIV Study", 32nd Aerospace Sciences Meeting and Exhibi, AIAA paper.
3. Majumdar, S and Rajani, B. N. (1999),"Numerical computation of Turbulent flow around Radome Structures", Engineering Turbulence Modelling and Experiments - Vol. 4, pp. 309-318.
4. Majumdar, S. and Rodi, W. (1989),"Three-Dimensional Computation of Flow past Cylindrical Structures and Model Cooling Towers", Building and Environment, Vol. 24, No. 1, pp. 3-12.
5. Norberg, C. (1987),"Effects of Reynolds number and a low-intensity free-stream turbulence on the flow around a circular cylinder", Dept. of Appl. Thermodynamics and Fluid Mech., Chalmers Univ. of Tech., Gothenburg, Sweden, Publ. No. 87/2.
6. Parammasivam, K. M. (2005),"Wind Tunnel Studies on Water Tank Tower with Terrain Simulation", Ph. D. Thesis, Anna University, Chennai.
7. Parammasivam K. M, Jayaraman K, Tamura Y, Matsui M, Yoshida A, (2005), "Wind loads on conical water tank towers in semi-urban terrains", The 6th Asia-Pacific Conference on Wind Engineering (APCWE-VI), pp.1774-1789.
8. Parammasivam K. M, Jayaraman K, Tamura Y, Matsui M, Yoshida A, (2005), "Wind directional effects on surface pressure distributions on conical water tank towers in semi-urban terrains", The 6th Asia-Pacific Conference on Wind Engineering (APCWE VI), pp.1736-1757.
9. Patankar, S. V. and Spalding, D. B. (1972),"A calculation procedure for heat, mass and momentum transfer n three-dimensional parabolic flows", International Journal of Heat and Mass Transfer, Vol. 15, pp.1787-1806.
10. Zhu, J, Rodi, W. and Schönung, B. (1989),"A Hybrid Differential-algebraic method for three dimensional grid generation", Technical Report, Institute for Hydromechanics, University Karlsruhe.

ABOUT THE JOURNAL

Aims

The aim of the Journal is a continuous and timely dissemination of research developments and applications. The Journal is an inter disciplinary forum for Wind and Engineering and publishes referred papers on the latest advances on the subject and their application to industrial wind engineering, wind induced disasters, environmental issues and wind energy. Papers on relevant and innovative practice and engineering application as well as those of an interdisciplinary nature are strongly encouraged. Discussions on any paper previously published in the Journal are also considered for publication. Articles submitted to the Journal should be original and should not be under consideration for publication elsewhere at the same time.
Besides regular issues containing contributed research papers, it will be the endeavour of the editors to bring out specialty issues covering a specific area of interest to include invited state-of-the-art papers.

Furthermore, short technical notes describing preliminary ideas on a proposed area of future research will also be considered for publication.

Members may also send news items, memoirs, book reviews for publication.

The Society is not responsible for statements and opinions expressed by the authors in the Journal.

Subscription

The journal will be brought out biannually. For ISWE members, subscription to ISWE Journal is included in the membership fee. The rates per issue for non-members are given below:

Regular Issue	: Rs. 150.00 (US$ 25.00, by air mail)
Special Issue	: Rs. 500.00 (US$ 50.00, by air mail)
Library Membership (Annual)	: Rs. 1000.00 (US $ 100.00 by air mail)

There are no page charges for the Journal of Wind and Engineering.
A copy of the journal will be sent by post to all corresponding authors after publication. Additional copies of the journal can be purchased at the author's preferential rate of Rs. 150.00 per Volume.

Preparation of the Manuscript

a. **Paper Length** : The length of paper should normally be restricted to 10 pages maximum.

b. **Headings and subheadings** : Headings should be in bold uppercase and not numbered. Sub- headings should be in bold lower case and may be numbered.

c. **Figures and Tables**: These should be numbered consecutively in Arabic numerals and should be titled. Figure captions should be given on a separate sheet. Figures should be very sharp.

d. **Photographs, Illustrations**: Good glossy bromide prints of these must accompany the manuscript and not be attached to the manuscript pages.

e. **References**: These should be listed alphabetically at the end of the text and numbered serially, cited in the text by the last name(s) of authors followed by the year of publication in parenthesis. In case of more than two authors, the last name of the first author followed by et al. and the year of publication is to be cited in the text. References are to be listed in he following format only:

1. Walker, G.R., Roy, R.J. 1985. Wind loads on houses in urban environment. Proc. of Asia Pacific Sym. on Wind Engg., University of Roorkee, Roorkee, India, Dec. 5-7.
2. Holmes, J.D., Melbourne, W.H. and Walker, G.R. A commentary on the Australian Standard for wind loads. Australian Wind Engineering Society, 1990.
3. Krishna, P., Kumar, K., Bhandari, N.M., (2005), "Review of Wind Loading Codes", A study sponsored by Gujarat State Disaster Management Authority, India.

f. **Abstract**: This should not exceed 150 words and be an abbreviated, accurate representation of the contents of the article. It should be followed by a list of 3 to 5 key words of these contents.

g. **Units**: All quantities should be in SI units. Other units may be enclosed in parenthesis after the SI units, if necessary.

Submission

Manuscript of the paper should be transmitted by e-mail, or, alternatively, the original manuscript together with a soft copy on CD should be submitted to the Editor-in-Chief / Editors for possible publication in the Journal.

Please make sure your contact address is clearly visible on the outside of all packages you are sending to the Editors.

Editorial Office: Located at : Office of Dr. A. K. Mittal, Scientist
Central Building Research Institute
Roorkee - 247667, INDIA, Tel: 01332- 283464
E-mail: iswe1993@gmail.com; achal_cbri@rediffmail.com
http://www.iswe.co.in

All enquiries may be addressed to the Editor-in-Chief / Editors Hon. Secretary, at this address.

Submitting a Paper to Journal

1. In order to maintain annonymity during any referring process, authors are requested to refrain from, or keep to a minimum, self-referencing.

2. In consideration of the publication of your Article, you assign us with full title guarantee, all rights of copyright and related rights in your Article. So that there is no doubt. This assignment includes the right to publish the Article in all forms, including electronic and digital forms, for the full legal term of the copyright and any extension or renewals. You shall retain the right to use the substances of the above work in future works, including lectures, press releases and reviews, provided that you acknowledge its prior publication in the Journal.

3. We shall prepare and publish your Article in the journal. We reserve the right to make such editorial changes as may be necessary to make the article suitable for publication; and we reserve the right not to proceed with publication for whatever reason. In such an instance, copyright in the Article will revert to you.

4. You hereby assert your moral rights to be identified as the author of the Article according to the Indian Copyright Designs & Patents Act.

5. You warrant that you have secured the necessary written permission from the appropriate copyright owner or authorities for the reproduction in the Article and the Journal of any text, illustration, or other material. You warrant that, apart from any such third party copyright material included in the Article, the Article is you original work, and cannot be construed as plagiarizing any other published work, and has not been and will not be published elsewhere.

6. In addition, you warrant that the Article contains no statement that is abusive, defamatory, libelous, obscene, fraudulent, nor in any way infringes the rights of others, nor is in any way unlawful or in violation of applicable laws.

7. You warrant that, wherever possible and appropriate, client or participant mentioned in the text has given informed consent to the inclusion of material pertaining to themselves, and that they acknowledge that they cannot be identified via the text.

8. If the Article was prepared jointly with other authors, you warrant that you have been authorized by all co-authors to sign this Agreement on their behalf, and to agree on their behalf the order of names in the publication of the Article.

THE INDIAN SOCIETY FOR WIND ENGINEERING

MEMBERSHIP FORM

Name : ..... Father's Name.....

Position : .....

Organisation:.....

Address.....

.....

Res. Address : .....

.....

Tel : .....Fax :.....

E-mail: .....

Nature of work and period of active involvement:

1. I/We wish to become the Individual/ Institutional member of the Indian Society for Wind Engineering (ISWE).
2. A Demand Draft for Rs. ..... payable to Indian Society for Wind Engineering at Roorkee as Membership fee is enclosed.

Date: Signature

Supported by:

Name	**Membership No.**	**Signature**
1.		
2.		

Please send this completed form to:

Hon. Secretary, Dr. A. K. Mittal
Central Building Research Institute, Roorkee - 247667, INDIA,
Tel: +91 1332- 283464
Mob: +91 9412074408
E-mail: iswe1993@gmail.com , achal_cbri@rediffmail.com
Website- http://www.iswe.co.in

OBJECTIVES OF THE INDIAN SOCIETY FOR WIND ENGINEERING

(a) The Society shall provide a necessary forum to the individuals and institutions connected with, or, interested in industrial aerodynamics, which includes wind effects on structures and buildings, land and sea transportation vehicles; mitigation of disasters due to cyclones, tornadoes, blizzards, sand storms, etc.; wind energy generation; study of atmospheric pollution and dispersion; and, related matters to come together and exchange ideas for the advancement and dissemination of knowledge in the field of Wind Engineering

(b) The Society shall promote research and development work in the field of Wind Engineering and shall maintain close liaison with the International Organizations working with allied objectives.

(c) The Society shall promote research results in professional practice.

(d) The Society shall make efforts to involve field engineers and professional organizations in its activities by arranging seminars, symposia, etc.

(e) The Society shall bring out a periodical publication.

(f) The Society shall institute awards and prizes to recognize excellence of research and application in Wind Engineering.

MEMBERSHIP OF THE SOCIETY

The Society shall have the following categories of membership:

(a) Individual (b) Institutional
(c) Honorary

Subscription: The life membership rates for different categories shall be as follows:

Individual Membership			
Indians and SAARC Nationals	Life	Rs.	1500.00
Other Foreign Nationals	Life	US$	100.00
Institutional Membership	Annual	Rs.	3,000.00
	Regular	Rs.	30,000.00

ISWE EXECUTIVE COMMITTEE

President	Dr. P. D. Porey	Director SVNIT, Surat
Vice-President	Dr. S. Arunachalam	Director Grade Scientist, SERC Chennai
Hon. Secretary	Dr. Achal Kumar Mittal	Scientist CBRI, Roorkee
Treasurer	Dr. Akhil Upadhyay	Asso. Prof. IIT, Roorkee
Members	Dr. Abhay Gupta	VP, Eigen, Noida
	Sh. Deepak Bansal	Asstt. Chief Projects, HUDCO, Delhi
	Dr. O. R. Jaiswal Asso.	Prof VNIT, Nagpur
	Sh. Ashok Kumar J. Shah	Prof. SVNIT, Surat
	Dr. (Mrs.) S. Selvi Rajan	Dy. Director, SERC Chennai
	Sh. Sanjay Kumar Varsheny	GM, Mahagun, Delhi
	Sh. T. N. Gupta	Former Executive Director, BMTPC Delhi
	G. S. Mandal	NDMA, Delhi

COMMUNICATION

Communication regarding change of address, subscription renewals, missed numbers, membership and Society Publications should be addressed to -

Dr. A. K. Mittal
Hon. Secretary
Indian Society for Wind Engineering,
Located at the Central Building Research Institute
Roorkee - 247667, INDIA
Tel: 01332- 283464
Mob: +91 9412074408
E-mail: iswe1993@gmail.com, achal_cbri@rediffmail.com
http://www.iswe.co.in

ISSN : 0973 - 0613

JOURNAL OF WIND & ENGINEERING

Vol. 6 No. 2 July 2009

CONTENTS

Published by: Indian Society for Wind Engineering, Located at Central Building Research Institute Roorkee 247667, INDIA, Tel: 01332- 283464, E-mail: iswe1993@gmail.com,http://www.iswe.co.in

Printed by : *R. K. Printers & Publishers, 26 Civil Lines, New Haridwar Road, Roorkee - 247667 Ph. : 270957, 9897276995*